CARRIER LIFETIME DYNAMICS OF EPITAXIAL LAYER HVPE GALLIUM ARSENIDE USING TIME-RESOLVED EXPERIMENTS

THESIS

Wayne E. Eikenberry, Captain, USAF

AFIT/GAP/ENP/06-03

DEPARTMENT OF THE AIR FORCE
AIR UNIVERSITY

AIR FORCE INSTITUTE OF TECHNOLOGY

Wright-Patterson Air Force Base, Ohio

AFIT/GAP/ENP/06-03

CARRIER LIFETIME DYNAMICS OF EPITAXIAL LAYER HVPE GALLIUM ARSENIDE USING TIME-RESOLVED EXPERIMENTS

THESIS

Presented to the Faculty

Department of Engineering Physics

Graduate School of Engineering and Management

Air Force Institute of Technology

Air University

Air Education and Training Command

In Partial Fulfillment of the Requirements for the

Degree of Master of Science (Applied Physics)

Wayne E. Eikenberry, BS

Captain, USAF

March 2006

AFIT/GAP/ENP/06-03

CARRIER LIFETIME DYNAMICS OF EPITAXIAL LAYER HVPE GALLIUM ARSENIDE USING TIME-RESOLVED EXPERIMENTS

Wayne E. Eikenberry, BS
Captain, USAF

Approved:

Lt Col Matthew J. Bohn (Chairman)	date
Michael A. Marciniak (Member)	date
Robert L. Hengehold (Member)	date

Abstract

GaAs is a potential semiconductor material for producing both mid-infrared and terahertz radiation using the new technique of quasi-phase matching in an orientationally patterned GaAs (OP-GaAs) crystal. OP-GaAs is grown using a fast growth process called hydride vapor phase epitaxy (HVPE), unfortunately, HVPE produces a high number of defects. These defects cause Shockley-Read-Hall recombination rates to dominate over Auger and radiative recombination rates.

The carrier lifetime from four GaAs samples are reported here using two different experimental techniques. The first experiment used a streak camera to measure the carrier lifetime via time-resolved photoluminescence. The temporal resolution of the streak camera can resolve the fast decay rate of the HVPE grown GaAs samples. The carrier lifetimes recorded by the streak camera for sample one is 8.5 ± 0.3 ps, sample two is 8.4 ± 0.3 ps, sample three is 11.3 ± 0.3 ps, and sample four is 10 ± 0.3 ps. The second experiment used time-resolved pump-probe reflectivity to measure the carrier lifetime. This experiment used two laser beams; one was to excite the sample and the other was to measure the change in the index of refraction caused by the carrier excitation. The carrier lifetimes obtained by the pump-probe experiment for sample one is 0.8 ± 0.2 ps, sample two is 2.1 ± 0.2 ps, sample three is 3.8 ± 0.2 ps, and sample four is 1.3 ± 0.2 ps. The results of the lifetimes of these two experiment methods differ with each other.

Acknowledgments

Working on this thesis has been the most challenging experience of my academic career. As a result, I feel a sense of accomplishment and have learned so much. This has been a wonderful opportunity for me and I will never forget my time here.

I am very grateful to the United States Air Force and to the Air Force Institute of Technology for allowing me to pursue my educational goals. I want to thank the committee members, Dr. Michael A. Marciniak and Dr. Robert L. Hengehold for their support, patience, and guidance. I want to express my gratitude to my advisor, Lt. Col. Matthew J. Bohn for his help and guidance throughout the entire thesis process. He was very patient with all of my questions and I learned a great deal from him. I also want to thank Dr. Walter Buchwald and Candace Lynch from Hanscom AFB, MA. They supplied the samples and gave me insight into what experiments they wanted accomplished.

Finally, I would like to thank my wife. It is because of her love, support, and encouragement that I was able to make it through the challenging times. Her motivation helped me to achieve my goals.

Table of Contents

List of Figures

Figure Page

List of Tables

CARRIER LIFETIME DYNAMICS OF EPITAXIAL LAYER HVPE GALLIUM ARSENIDE USING TIME-RESOLVED EXPERIMENTS

I. Introduction

Background

Infrared technologies have played an important part in military and civilian applications, yet the mid-infrared and terahertz capabilities have not been fully realized. A possible semiconductor, Gallium Arsenide (GaAs) grown under certain conditions, might be able to produce a mid-infrared OPO and terahertz radiation from either a P.C. or difference frequency mixing. Four GaAs samples were supplied from the Air Force Research Laboratory (AFRL)/ Sensors Directorate Electromagnetic (SNHC) at Hanscom AFB, MA. These samples were produced by a method of growing thick epitaxial layers of GaAs by low pressure hydride vapor phase epitaxy (HPVE) [20]. Carrier lifetime was measured to assess the suitability of the unique thick layers for photomixing and ultra-short current pulse generation.

Problem Statement

AFRL/SNHC, Hanscom AFB, MA has developed a new fast growth technique for GaAs. The goal in this experiment is to measure the carrier lifetime from four samples of GaAs using two different time-resolved experimental techniques.

Research Objectives

To better assess the applicability of GaAs as a terahertz source, the carrier recombination rates of GaAs need to be determined. The streak camera was the first experiment used to measure the carrier recombination rates through time resolved photoluminescence. The second experiment involved the time resolved pump probe reflectivity technique to find the carrier lifetime.

Methodology

For both experiments, an ultra short pulse laser was used to excite four different GaAs samples. The time resolved photoluminescence was recorded on a streak camera and analyzed to determine the carrier lifetime. The time resolved pump probe reflectivity technique was used to measure the change in reflectivity of the sample in order to determine the carrier lifetime. The data from both techniques was modeled to find the carrier lifetime and comparison between the two techniques were made.

Implications

If the carrier lifetimes are very short, such as a picosecond or shorter, then GaAs can be used for the generation and detection of terahertz radiation. There are many promising military and non-military applications for the use of terahertz radiation. Some possible areas are: mine detection, explosives type determination, personnel and package inspection, target identification, forensic science, and astronomy. In mine detection, the beams pass through the covering material where objects beneath can be easily detected. It does not matter if the mines are made of wood, plastic, or metal; terahertz detection will reduce false positives in detecting mines. Terahertz can be used to detect the

different absorption lines in explosives, therefore, determining the type of explosive [8]. Terahertz detection also plays a major role in security because terahertz radiation has lower photon energy than X-rays, therefore, allowing safe exposure for personnel and providing greater spectral resolution and greater penetration of the object being scanned [9].

II. Background

Semiconductors resemble a poor insulator more than an imperfect metal. In a metal, the energy gap between the valence and conduction band does not exist, whereas an insulator requires a high thermal excitation for electrons to reach the conduction band. The band gap, also called the forbidden energy region, has certain applicable physical properties between a filled valence band and an empty conduction band. It can be greatly altered by adding impurities into the lattice, changing the electrical conductivity properties. Impurities can be ions that replace the normal atoms in the lattice or they can be a high number of defects in the lattice structure.

There is no such thing as a pure semiconductor, but one is considered pure if its concentration of impurities is less than one in one billion. A pure semiconductor is an intrinsic semiconductor; whereas an extrinsic semiconductor has many impurities throughout its lattice. Many semiconductors, such as silicon, come from Column IV of the periodic table and are used in electronic devices and microcircuits, while others come from the III-V Columns, such as GaAs and are used in optoelectronic devices. The Column IV materials form a diamond crystal structure, whereas GaAs forms in a zincblend structure similar to a diamond structure except two different ions are present, as illustrated in Figure 1.

Band Gap

The band gap is significant in all semiconductors and is important in GaAs. The energy band gap of GaAs is 1.43 electron-volts (eV). A photon of energy equal to or greater than the band gap energy, E_g, can excite the electron from the valence band to the

conduction band by creating an electron-hole pair. If the photon's wavelength is longer than $\hbar c / E_g$, where $\hbar$ is Planck's constant and, c, is the speed of light, there will not be enough energy to excite the electron from the valence band to the conduction band and it will pass through the semiconductor without being absorbed.

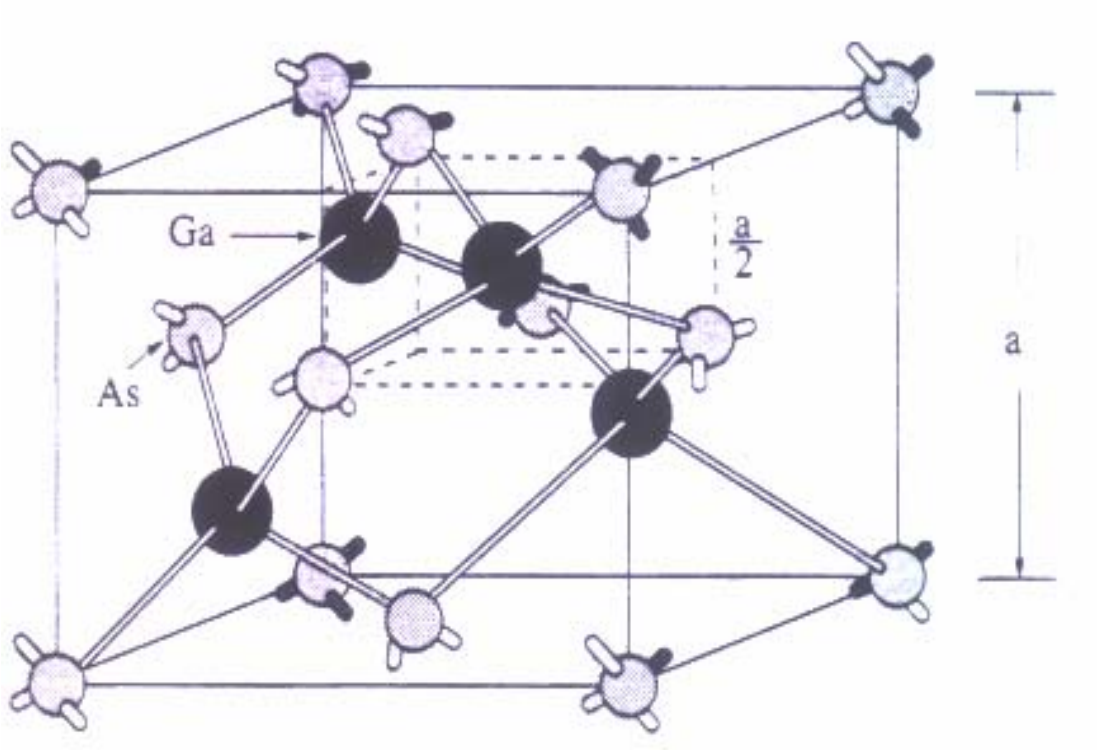

Figure 1. Zincblend structure for GaAs where $a = 5.65\,\text{Å}$ [1:12]

In GaAs and other III-V semiconductor materials, the band gap energy is defined as the energy difference between the minimum of the conduction band and the maximum of the valence band as shown in Figure 2. The top of the valence band occurs at zero momentum (k). When the bottom of the conduction band is also at k = 0, a direct band gap semiconductor forms. A direct band gap is at the center of the Brillouin zone (k = 0) [2:426], and does not require a change in momentum to decay, therefore, it has a much greater probability of emitting a photon (radiative recombination). In an indirect band

gap, the conduction band minimum is not at k = 0 and the valance band maximum is at k = 0, therefore, a change in momentum is required for a photon to be emitted.

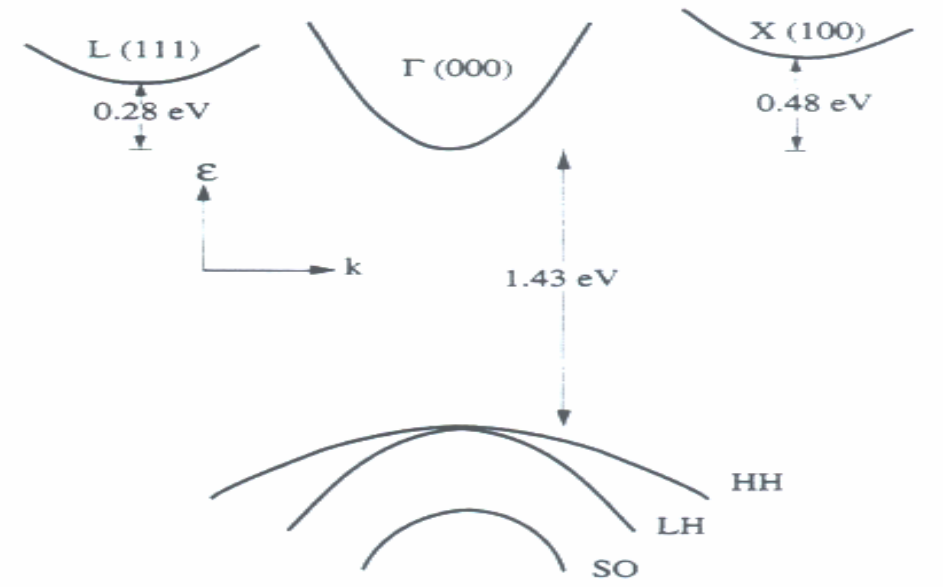

Figure 2. Direct band gap of GaAs where the valence band electron is at a maximum and the conduction band electron is at a minimum [1:64]

Electron and Hole Carrier Concentration

Electron density is observed to be greatest at the bottom of the conduction band and decreases as temperature increases [2:385]. The carrier concentrations can be described by the density of states, Fermi-Dirac distribution, temperature, the band gap structure and the purity of the semiconductor crystal.

Carrier concentration, also known as carrier density of electrons, is represented by n_0 and for holes, p_0. They are derived by the equations

$$n_0 = \int_{\varepsilon_c}^{\infty} f(\varepsilon) g_c(\varepsilon) d\varepsilon \qquad [1]$$

and

$$p_0 = \int_{-\infty}^{\varepsilon_v} f_p(\varepsilon) g_v(\varepsilon) d\varepsilon \qquad [2]$$

where, $f(\varepsilon)$, is the Fermi-Dirac distribution for electrons, $g_c(\varepsilon)$, is the density of states for the conduction band, $g_v(\varepsilon)$, is the density of states for the valence band, ε_c, is the energy level of the conduction band, ε_v, is the energy level of the valence band, and, $f_p(\varepsilon)$, is the Fermi-Dirac distribution for holes. The Fermi-Dirac distribution, $f(\varepsilon)$, is defined as

$$f(\varepsilon) = 1/(1 + e^{(\varepsilon - \varepsilon_f)/kT}) \qquad [3]$$

and, $f_p(\varepsilon)$, is

$$f_p(\varepsilon) = 1 - f(\varepsilon) \qquad [4]$$

where, ε_f, is the Fermi energy. The Fermi energy of an intrinsic semiconductor can be

$$\varepsilon_f = \frac{1}{2}(\varepsilon_c + \varepsilon_v) + \frac{3}{4} k_B T \ln \frac{m_p^*}{m_n^*} \qquad [5]$$

where, *T*, is the temperature and

$$\frac{1}{2}(\varepsilon_c + \varepsilon_v) \qquad [6]$$

is the half way point for the band gap energy. The density of states per unit volume is defined for the electrons in the conduction band as [2:385]

$$g_c(\varepsilon) d\varepsilon = \frac{8\sqrt{2\pi}}{h^3} m_n^{*3/2} \sqrt{\varepsilon - \varepsilon_c}\, d\varepsilon \qquad [7]$$

and for holes in the valence band as

$$g_v(\varepsilon) d\varepsilon = \frac{8\sqrt{2\pi}}{h^3} m_p^{*3/2} \sqrt{\varepsilon_v - \varepsilon}\, d\varepsilon \qquad [8]$$

where, m_n^*, is the effective mass of the electron, m_p^*, is the effective mass of the hole, and, *h*,

is Planck's constant which is a combination of the heavy hole and light hole

$$m_h^{*3/2} = m_{lh}^{*3/2} + m_{hh}^{*3/2}. \quad [9]$$

Figure 3 illustrates how the density of states relates to the valence and conduction band in a semiconductor. Further, the product of the electron and hole is equivalent to the intrinsic carrier concentration, n_i, squared

$$n_0 p_0 = n_i^2 \quad [10]$$

and

$$n_i = 2\left(\frac{2\pi\sqrt{m_n^* m_p^*}k_B T}{h^2}\right)^{3/2} e^{-\Delta\varepsilon/2k_B T}. \quad [11]$$

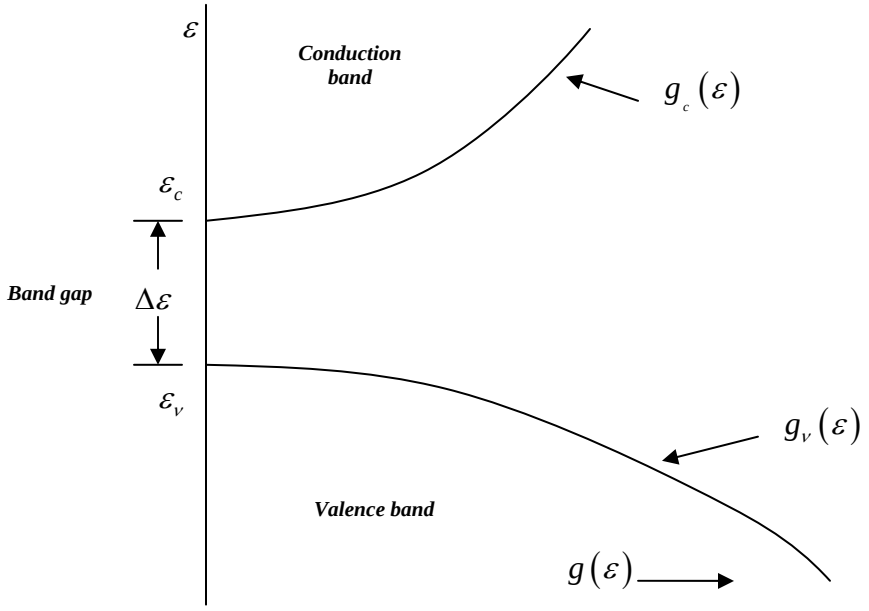

Figure 3. Density of states relates to the valence and conduction band in a semiconductor [2:386]

Impurities

Some impurities will always exist in the semiconductor, therefore, there is no such thing as a pure (intrinsic) semiconductor. No matter how well the growth process is conducted, one can never produce a completely pure crystal. The four GaAs samples were never doped in the growth process; therefore, impurities will be low in concentration and will not affect decay rates. If shorter lifetimes are required, then doping is an option to increase the decay rates.

Temperature

At absolute zero Kelvin, intrinsic semiconductors are perfect insulators, but as the temperature increases, the electrons begin to cross the band gap into the conduction band, increasing the electric conductivity. The electrons leave the unoccupied states allowing hole conduction to begin in the valence band. The band gap is much larger than $k_B T$ at normal temperatures, where, $k_{B,}$ is the Boltzmann constant. As temperature increases, the electron population in the conduction band increases exponentially; this in turn increases the electrical conductivity exponentially, therefore changing the properties of the band gap.

In a solid the phonon energy is associated with temperature; as temperature increases, the vibrational energy increases, therefore, phonon energy increases. Energy in a solid is associated with the vibration of atoms in the lattice. The vibrational energies of atoms are quantized and are treated as quantum harmonic oscillators. The quantum harmonic oscillators gain and release small amounts of energy $\hbar\omega$. These small amounts of energy are called phonons and behave similarly to photons of electromagnetic energy.

Phonon energy greater than the band gap can form electron-hole pairs, but the probability of this happening for GaAs at room temperature is very rare because the phonon energy for GaAs is 0.036 electron-volt and the band gap energy for GaAs is 1.43 electron-volt at room temperature.

Temperature affects the band gap in a semiconductor; as temperature increases, the lattice expands. The dependence of temperature on the band gap for GaAs follows the equation [1:68]

$$E_g(T) = E_g(0) - \frac{\alpha T^2}{T + \beta} \qquad [12]$$

where, $E_g(0)$, is the band gap energy at 0 Kelvin and, α, and, β, are constants (see Figure 4). The constant, α, for GaAs is 5.405×10^{-4} eV/k^2, for, β, is 204 0^o Kelvin, and for $E_g(0)$ is 1.519 eV [1:68].

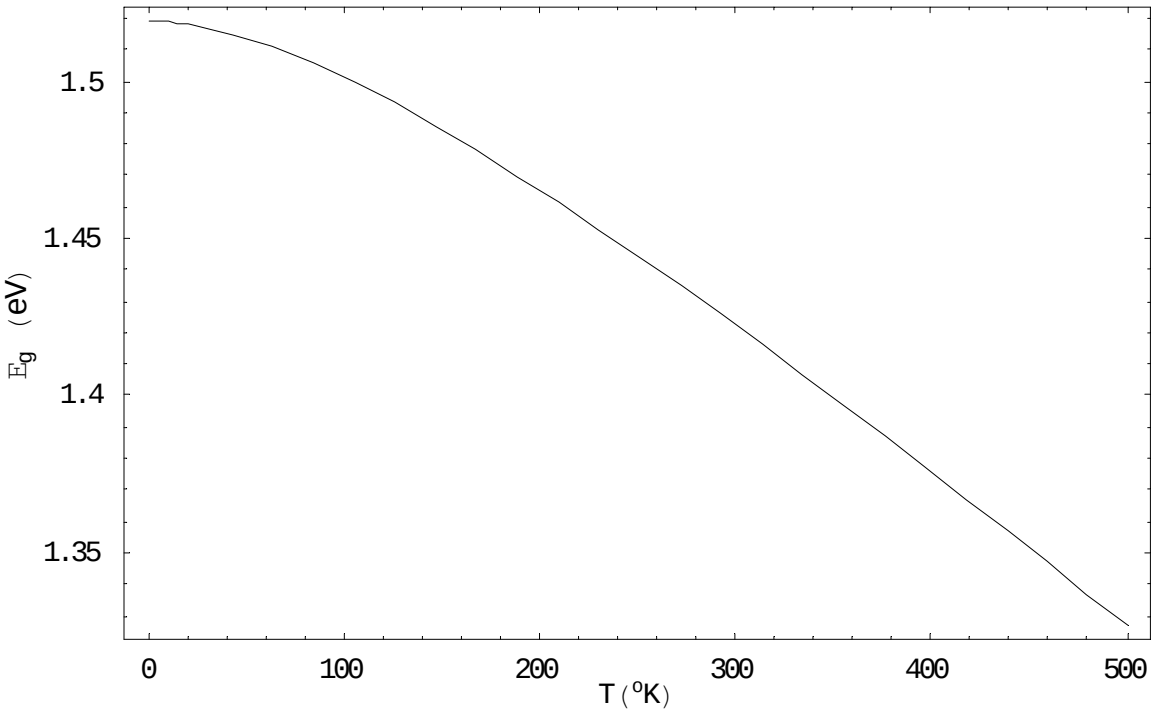

Figure 4. Temperature effects on band gap for GaAs from equation [12]

Recombination

The process of an electron-hole recombination is based on the creation and destruction of electron-hole pairs. The electron-hole pairs are created by photons hitting the crystal structure and their energy being absorbed if it is equal to or greater than the band gap energy. The opposite of absorption is the process of the electron-hole pair recombining. There are two types of recombination; radiative and non-radiative. The non-radiative recombination occurs when excessive energy is released as phonons or as excess kinetic energy in an additional electron and dissipated as heat. Radiative recombination occurs when the energy is released as photons. Photoluminescence is the result of electron-hole radiative recombination after the injection of photons on the crystal sample from an outside source, such as a laser [1:114].

The carrier recombination with no external source normally occurs at a constant rate due to thermal equilibrium. When the semiconductor is pumped from an outside source, such as a continuous wave (cw) laser, a new equilibrium is established where the electron-hole recombination rate is a constant. The non-equilibrium electron-hole concentration follows

$$n = \Delta n + n_0 \text{ and } p = \Delta n + \frac{n_i^2}{n_0} \qquad [13]$$

where, n_0, is the equilibrium concentration for electrons and, Δn, is the electron-hole pairs with a recombination rate

$$R = R_r = B_r np = B_r n_i^2 \qquad [14]$$

where, B_r, is the probability for band-to-band recombination [3:111]. When the excitation source is turned off, the electron-hole recombination rate returns to its

equilibrium state, n_0, and, p_0, . The excess carriers decay back to the valence band at a rate following $\exp(-t/\tau)$ where, τ, is the lifetime of the carriers. The total carrier lifetime for radiative and non-radiative recombination is

$$\frac{1}{\tau} = \frac{1}{\tau_r} + \frac{1}{\tau_{nr}} \qquad [15]$$

where, τ_r, is the radiative lifetime and, τ_{nr}, is the non-radiative lifetime.

Auger

The Auger effect is a process where an electron recombines with a hole and imparts its recombination energy to another electron. In turn, the electron releases its excess energy into the lattice. Because of this electron to electron interaction, the Auger effect should increase as carrier concentrations increase. Since an increase in temperature causes carrier concentrations to increase, the Auger effect has to increase as temperature increases. This effect can be represented as

$$\tau_{Auger} \propto \left(\frac{E_g(T)}{k_B T}\right)^{3/2} \exp\left(\frac{1+2M}{1+M}\frac{E_g(T)}{k_B T}\right) \qquad [16]$$

where, τ_{Auger}, is the electron-hole lifetime due to the Auger effect and, *M*, is the ratio of the effective mass for the electron, m_e^*, and the hole, m_h^*, which if $m_e^* < m_h^*$, then $M = m_e^*/m_h^*$ and if $m_e^* > m_h^*$, then $M = m_h^*/m_e^*$ [3:162]. If Δn in equation [13] is small and, n_i^2, is fairly negligible compared to carrier concentration, the rate, *R*, due to Auger can be expressed as

$$R = \frac{n}{\tau} = C_{Auger} n^3 . \qquad [17]$$

Shockley-Read-Hall

In intrinsic semiconductors, absorption and emission of photons occur close to the band gap energy, but in a semiconductor with higher defects, photon emission decreases and phonon emission increases. During the growth process, defects can form as impurities substituting the atoms in a crystal lattice. While other defects, such as vacancies of atoms in a lattice, interstitial atoms located in a non-lattice site, or a multiple combination of the previously mentioned, can form deep levels in the band gap [1:103]. These deep levels exist in the band gap and essentially trap electrons as they move from the conduction band to the valence band as shown in Figure 5. The deep levels or traps prevent the full recombination across the band gap. Instead, the recombination that would otherwise create a photon creates a phonon via a non-radiative recombination. These defects or traps are described by the Shockley-Read-Hall theory of recombination. When an electron tries to recombine with the hole in the valence band, it is captured by the trap called an electron capture. In the electron emission, the electron is released back into the conduction band. The same process occurs for the holes in the valence band. HVPE grown GaAs has many defects; therefore Shockley-Read-Hall should dominate in carrier recombination.

Shockley-Read-Hall Recombination Rate

Shockley-Read-Hall recombination rate can be expressed as

$$R_{SRH} = S_r v_{th} N_T \frac{np - n_i^2}{n + p + 2n_i^2 \cosh\left(\frac{\varepsilon_T - \varepsilon_{Fi}}{k_B T}\right)} \quad [18]$$

where, S_r, is the cross section of the recombination center, ν_{th}, is the thermal velocity of the carriers, N_T, is the concentration of the traps and, ε_T, is the energy position of the trap level [1:105]. For intrinsic material, it can be assumed that $p = n$ and that defects behave as true recombination centers, therefore, $\varepsilon_T = \varepsilon_{Fi}$, which in turn, the cosh term goes to one. Since the samples are not doped, n_i, is approximately zero, then equation [18] can be simplified to

$$R_{SRH} = S_r \nu_{th} N_T n . \qquad [19]$$

Further simplification of equation [19] can be accomplished by setting $A_{SRH} = S_r \nu_{th} N_T$ and the final expression for Shockley-Read-Hall recombination rate is [1:105]

$$R_{SRH} = \frac{n}{\tau} = A_{SRH} n . \qquad [20]$$

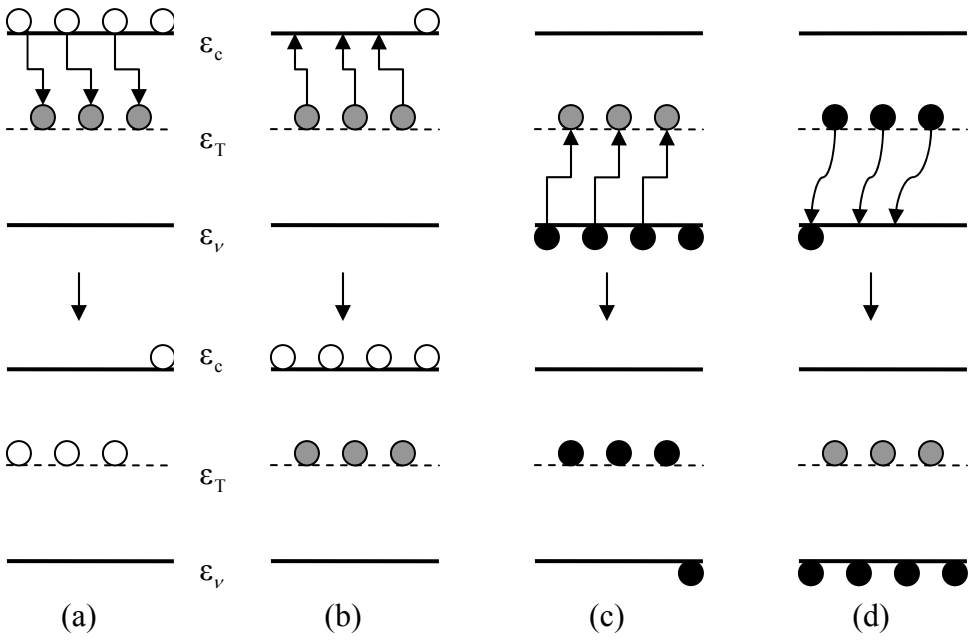

Figure 5. Traps in the band gap do to defects, (a) electron capture, (b) electron emission, (c) hole capture, (d) hole emission [1:103]

Recombination Rate

The carrier density excited from the energy of an optical excitation pulse, E_p, in a semiconductor can be determined from the number of photons striking the sample. The number of photons from the excitation pulse is given by

$$N_{ph} = \frac{E_p}{\hbar\omega}. \qquad [21]$$

Some of the photons from the excitation pulse incident on the surface of the material will be reflected off of the sample and is expressed as (1-R). The remaining excitation pulse is absorbed into the semiconductor material with an absorption coefficient, α. The absorption coefficient can be determined by

$$\alpha(\hbar\omega) = \frac{C_1}{n_r}\left(\frac{2m_r^*}{m_0}\right)^{3/2}\left(\frac{f_{cv}}{\hbar\omega}\right)\left(\hbar\omega - \mathcal{E}_g\right)^{1/2} \qquad [22]$$

where,

$$C_1 = \frac{q^2 m_0^{1/2}}{4\pi\hbar^2 \in_0 c} \qquad [23]$$

and

$$f_{cv} = 2\frac{\left|\rho_{cv}^2\right|}{m_0} \qquad [24]$$

where, m_0, is the rest mass of the electron and, $\in_0$, is the permittivity. In GaAs, f_{cv}, is 23 electron- volts and is the oscillation strength for the transition [1:124], $\left|\rho_{cv}^2\right|$, is the average squared matrix element for the transition between the Block states in the valence

and conduction bands [17:7804], n_r, is the index of refraction of the material and, *c*, is the speed of light. Equation [22] can be further simplified for GaAs as shown [1:124]

$$\alpha(\hbar\omega) = 5.6\text{x}10^4 \frac{(\hbar\omega - \mathcal{E}_g)^{1/2}}{\hbar\omega} \quad (\text{cm}^{-1}). \tag{25}$$

The total number of carriers produced from an excitation pulse is given as

$$N_{total} = \frac{E_p}{\hbar\omega}(1-R). \tag{26}$$

The beam width from the excitation pulse only strikes a certain area of the sample unless the sample is completely engulfed in the beam. The volume of illumination, *V*, is expressed as [18:70]

$$V = \frac{\pi\omega_0^2}{\alpha}, \tag{27}$$

where, ω_0, is the radius of the Gaussian shape of the laser pulse which represents 86% of that shape or at e^{-2} and, α, is the absorption coefficient. The carrier density generated from the excitation pulse of radius, ω_0, onto the sample is given as

$$n(t) = \frac{E_p}{\hbar\omega}(1-R)\frac{1}{V}. \tag{28}$$

The total carrier recombination rate can be expressed as

$$-\frac{dn}{dt} = A_{SRH}n + B_{rad}n^2 + C_{Aug}n^3 \tag{29}$$

with the coefficients determined earlier. If the semiconductor has many defects, the Shockley-Read-Hall effect will dominate in the carrier recombination rate, and the Auger

and the radiative recombination will be negligible [14:2335]. The approximation of equation [29] can be rewritten as

$$-\frac{dn}{dt} = A_{SRH} n \qquad [30]$$

and the new solution for carrier concentration is

$$n = n_0 \mathrm{e}^{-A_{SRH} t}. \qquad [31]$$

Another way to curve fit the data is to use two exponential expressed as

$$n(t) = (1 - e^{-t/\tau_1}) e^{-t/\tau_2}. \qquad [32]$$

The first exponential in equation [32] represents the initial increase due to carrier cooling, τ_1, and the second represents the carrier lifetime, τ_2. The carrier cooling will be further explained at the streak camera data and analysis section and why equation [32] was chosen.

III. Experimental Procedures and Setup

There were two different types of experiments carried out on the HVPE grown GaAs samples. The first experiment was the time-resolved photoluminescence (TRPL) using a streak camera. The second experiment was the time-resolved pump probe reflectivity (TRPPR).

TRPL Streak Camera Setup

The setup began with a three part laser system as shown in Figure 6. The first part of the system consists of an Nd:YVO_4 laser called a Verdi from Coherent. This laser is fairly new and has a pump power up to 16 watts emitting at 528 nanometers. The Verdi laser pumps a Coherent Mira 900, which is a Ti:Sapphire laser with mode locking capabilities, operating in the 790-910 nanometers with an average power

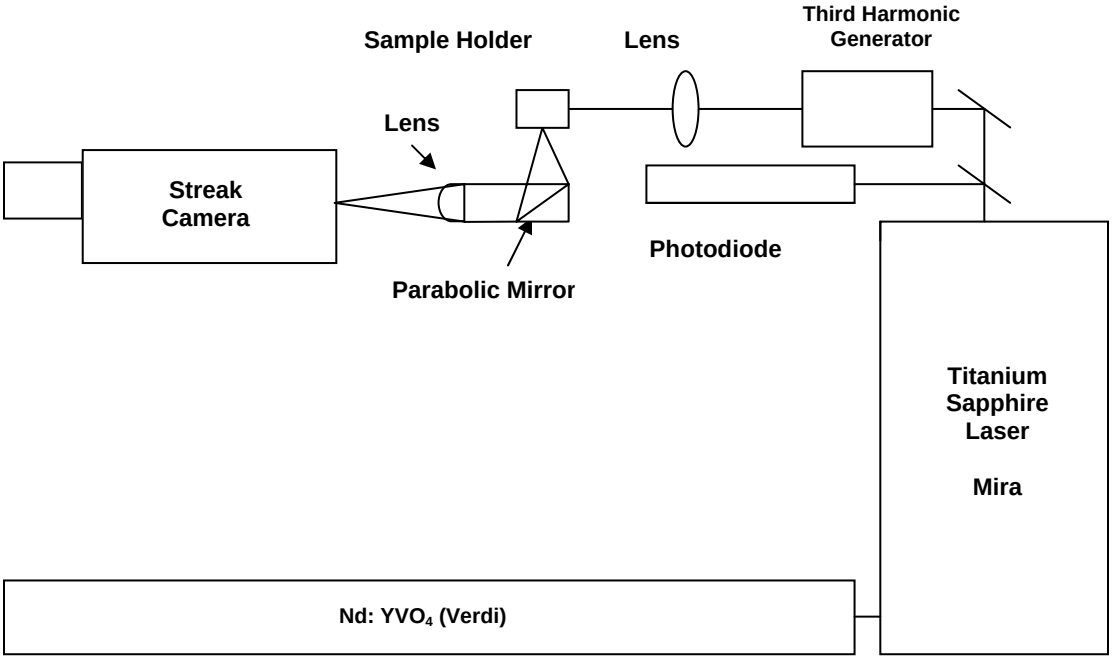

Figure 6. Time-resolved photoluminescence with a streak camera setup

output of 1100 milliwatts with a 12-14 watt pump laser. The mode locking capabilities of the Mira allow it to be pulsed instead of operating as a continuous wave (cw) laser. The Mira pulse repetition rate is 76 megahertz with a pulse width of about 100-femtoseconds. The peak power of the pulse is 100 kilowatts using a 12-14 watt pump laser. The autocorrelation pulse width of the Mira 900 measured by an autocorrelator is not the same value as the actual pulse from the Ti:Sapphire. The actual pulse is found by multiplying a factor of 0.684, so a 150 femtosecond autocorrelation will give an actual pulse width of 103 femtoseconds.

The third part of the laser system is called a third harmonic generator (THG). The THG is an Inrad MIN 5-050 ultra-fast harmonic generation system. The second harmonic generation (SHG) part of the THG was used and will be referred to as a SHG. The SHG produces the second harmonic generation through a non-linear crystal and creates a frequency-doubled beam at approximately 415 nanometers. The reason for using the SHG is so that the 415 nanometers laser pulse can be easily removed with a long pass wavelength filter from the photoluminescence. Without the SHG, the Ti:Sapphire lases at 830 nanometers, much too close to the luminescence wavelength of the GaAs at 875 nanometers, allowing possible contamination from the pump light into the streak camera, especially when a spectrometer is not being used in the setup.

The SHG is the process of sending two identical wavelength beams through a non-linear crystal at the same time. The polarization effects of a single beam through anisotropic or non-linear medium is

$$P = \in_0 \chi E_0 \sin \omega t + \in_0 \chi_2 E_0^2 \sin^2 \omega t + \in_0 \chi_3 E_0^3 \sin^3 \omega t + \cdots \qquad [33]$$

where, χ, is a dimensionless susceptibility constant for each order [6:640], E_0, is the electric field for each order and, $\in$, is the dielectric constant for each order. If two identical frequency beams at, ω, transit through the non-linear crystal at the same time, the second order component of equation [33] becomes

$$P_2 = \in_2 \chi_2 (E_{01}^2 \sin^2 \omega t + E_{02}^2 \sin^2 \omega t + 2E_{01}^2 E_{02}^2 \sin \omega^2 t) \quad [34]$$

where, χ_2, is a dimensionless second order susceptibility constant and, P_2, is the second order component of the electric polarization. This, in turn, creates a third beam that is doubled in frequency of the original; therefore, with a pump beam at 830 nanometers, the beam is doubled to 415 nanometers.

The beam exits the SHG and is focused through a CaF_2 lens with a 150 millimeters focal length. A CaF_2 is used because the beam does not cause the lens to fluoresce in the near infrared causing possible unwanted light into the streak camera. The beam's diameter out of the SHG is approximately 7 millimeters and diverges to 9 millimeters at the CaF_2 lens. A short-pass filter allows only the 415 nanometers wavelength to pass so the 830 nanometer wavelength is stopped before the sample. When the 830 nanometer beam is doubled to 415 nanometers, some of the 830 nanometer light is still present in the beam.

The sample sits on a three-axis translation stage placed at an angle greater than 45 degrees. This prevents the reflected pump beam from being focused into the streak camera. The photons due to excitation from the sample are captured by a parabolic mirror that has a three-axis translation stage and has vertical and horizontal tilt ability. This allows for fine tuning the collected photons onto the streak camera slit. The

collected photons are focused through a lens with a 150 millimeter focal length which makes a spot size approximately 50 ± 10 microns. The streak camera can be further aligned to allow maximum throughput of light with the minimum slit width possible. The streak camera measures the intensity as a function of time. The SHG emits an 830 nanometer beam that was not doubled in wavelength through a second port, and this beam is used for the autocorrelator and the synchronization diode for the streak camera.

Streak Camera Operation Process

In the first part of the experiment, Hamamatsu C6860 Synchroscan streak camera was used. The streak camera has been used in the past for shorter wavelength samples such as GaN, but GaAs emits in the near infrared region around 830 nanometers wavelength range. The streak camera has an S-20 sensor head as shown in Figure 7. The spectral response of the camera at the 830 nanometer wavelength falls within the range for the S-20 sensor head in Figure 7.

The streak camera's operation takes light and converts it into an image. The light enters the streak camera through a horizontal slit. The slit image of the light sample is focused onto a photocathode on the streak tube as shown in Figure 8. The photons that strike the photocathode are converted into electrons which are emitted and accelerated by a strong electrostatic field onto a micro channel plate. Two sweep electrodes, also called deflection plates, sweep the path of the electrons in the chamber. The deflection plates create a varying voltage across the electron path causing the electrons to move perpendicular to the slit width located at the entrance of the streak tube. These electrons then exit the micro channel plate (MCP) and bombard the phosphor screen and are read

by a signal processor. The electrons are then converted into an optical image called a streak image.

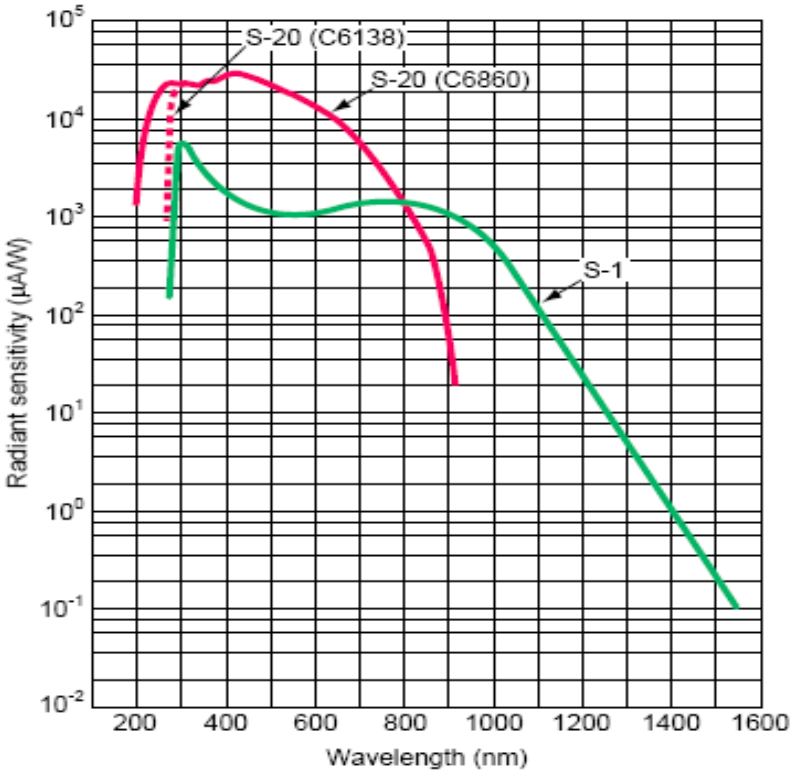

Figure 7. Spectral response characteristics for the streak camera S-20 (C6860)

Arriving at different times, the electrons will have different vertical positions on the phosphor screen. Therefore, the time axis of the incident light corresponds to the vertical axis on the image screen and the intensity of the incident light can be determined by the density of the image. It is necessary for the timing of the deflection to be synchronized with the time the electrons arrive in the deflection field. This is done by a trigger signal where the incident light is focused onto a photodiode to generate a signal for the deflection plates. Varying the voltage in the deflection plates can help determine photoluminescent events that can be temporally separated. The streak camera is limited

in its temporal resolution, and if the decay rates of the sample are too fast, then the camera will not be able to resolve the luminescent decay.

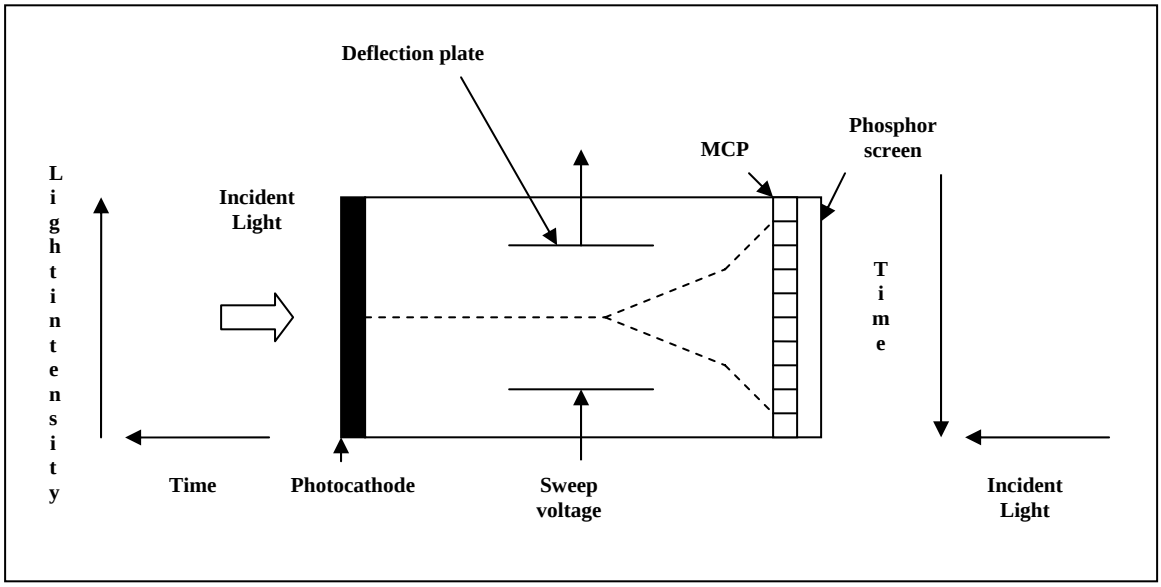

Figure 8. Streak camera operation process

Experimental Analysis for Streak Camera

The goal of this experiment was to find the lifetime of four HVPE grown GaAs samples using two different experimental techniques and to compare the results. The first technique used a streak camera, which was a difficult process to setup but could be accomplished fairly easily once the setup was complete. The streak camera is a good method for measuring lifetime using the time resolved process, but it is only accurate to approximately 0.5 picoseconds without laser jitter [13].

Spectrometer

Originally the TRPL was setup with the streak camera attached to a spectrometer with a photo multiplier tube (PMT) as shown in Figure 9. In the previous experiment, the

helitran (sample housing designed for low temperature experiments) was suspended from the lab table overhead, so the laser path had to be raised to the level of the sample. The previous experimentalist, Jost [4:60], had difficulty keeping the streak camera aligned because it was suspended on jacks, which would slightly settle over time. This caused resolution problems in the streak camera where the full width at half maximum (FWHM) of the laser pulse was broader than the stated specification. The results of the stated and measured FWHM of the laser pulse will be given later in this section.

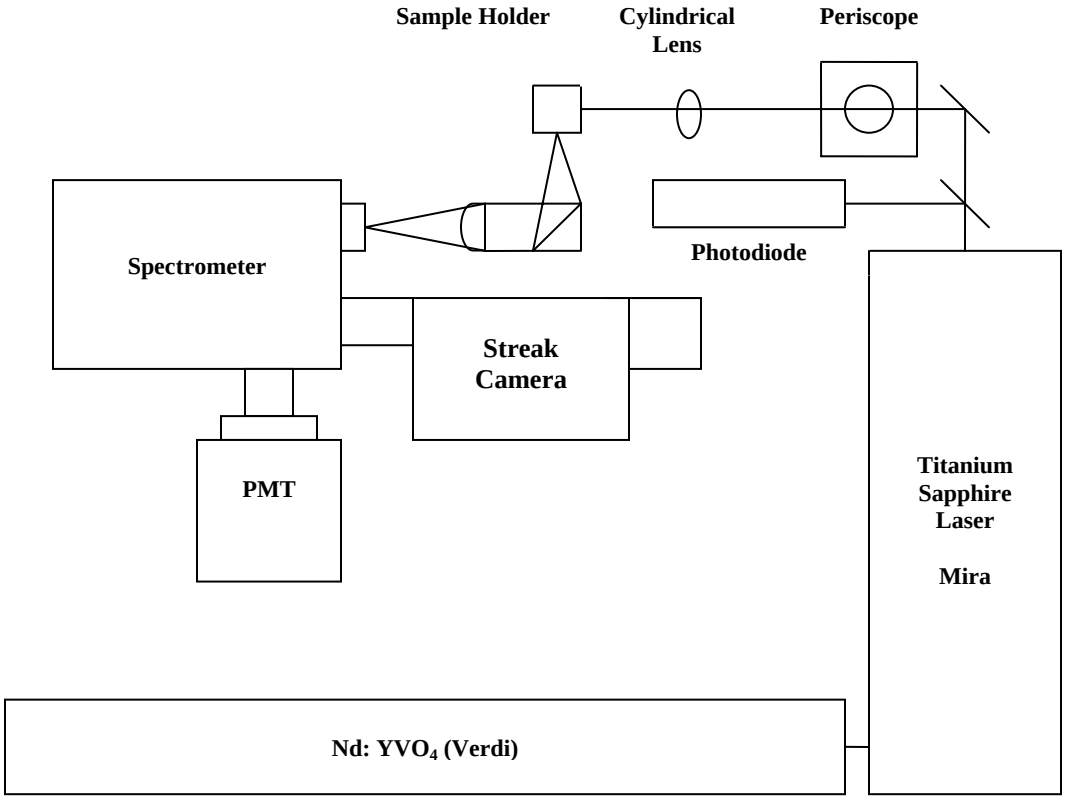

Figure 9. Original setup for the TRPL

The spectrometer was calibrated using a mercury lamp, ensuring spectral accuracy with well known published results. Any minor adjustments that needed to be made were accomplished at this point to ensure wavelength accuracy. The streak camera

was calibrated following Jost's alignment procedures [4:80] with the mercury spectrum through the spectrometer and compared with the streak camera and PMT. The GaAs sample was placed into the helitran and using the spectrometer, photoluminescence data was taken. The results from the spectrometer are shown in Figure 10 and it can be noticed that around 830 nanometer, the laser pump's spectral peak can be seen. The GaAs photoluminescence peaks at the band gap, given by, $\lambda_g = hc/\varepsilon_g$ where hc = 1240 electron-volts-nanometers and λ_g = 873 nanometers.

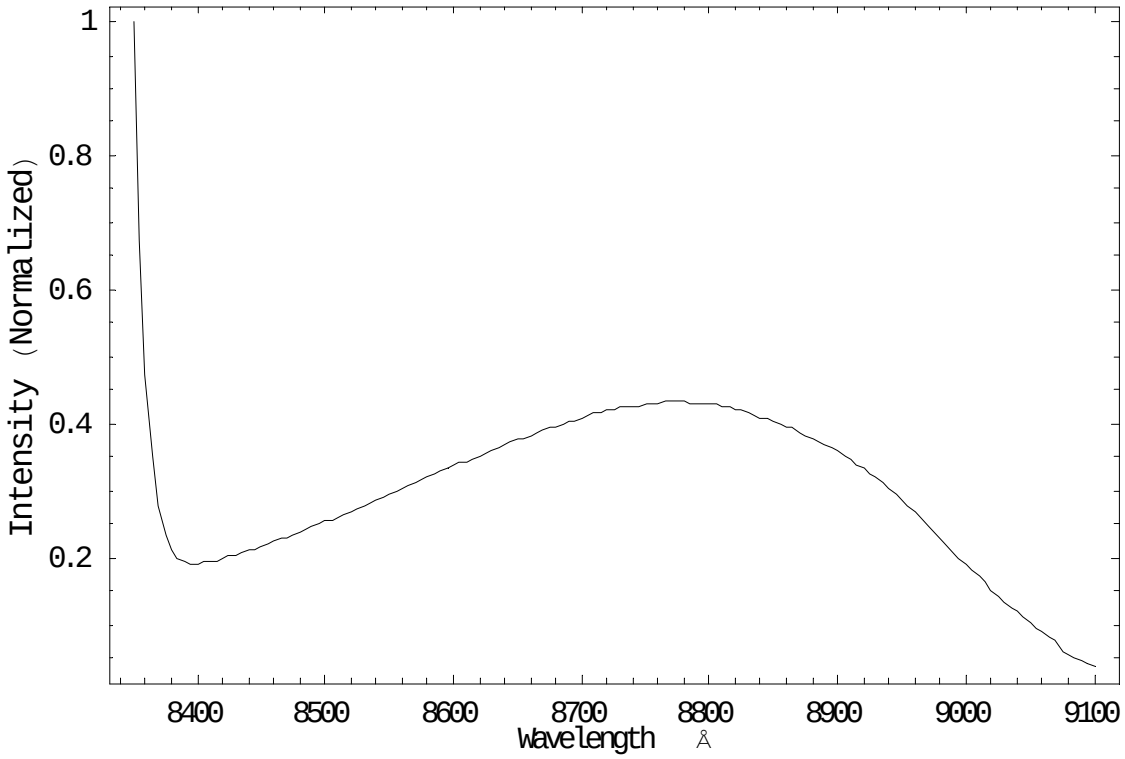

Figure 10. Intensity as a function of wavelength of GaAs illuminated at 830 nanometers

The SHG was originally bypassed using a periscope and the sample was illuminated with the 830 nanometers laser pump. The SHG was used to eliminate any possible effects from the laser pulse contaminating the streak camera data. This would

have a much greater effect when the spectrometer was removed from the streak camera setup.

Through the process of producing a second harmonic beam, the 415 nanometers beam still contains some of the original 830 nanometers light. This can be easily filtered out with a short pass wavelength filter. The shorter wavelength beam is used to excite the sample to get the same results; also, the scattered 415 nanometers light can be filtered using a low pass filter on the streak camera. The GaAs spectral maximum is around 870-880 nanometers and has a broad peak as shown in Figure 11. Now that the wavelength is known, temporal measurements can be obtained.

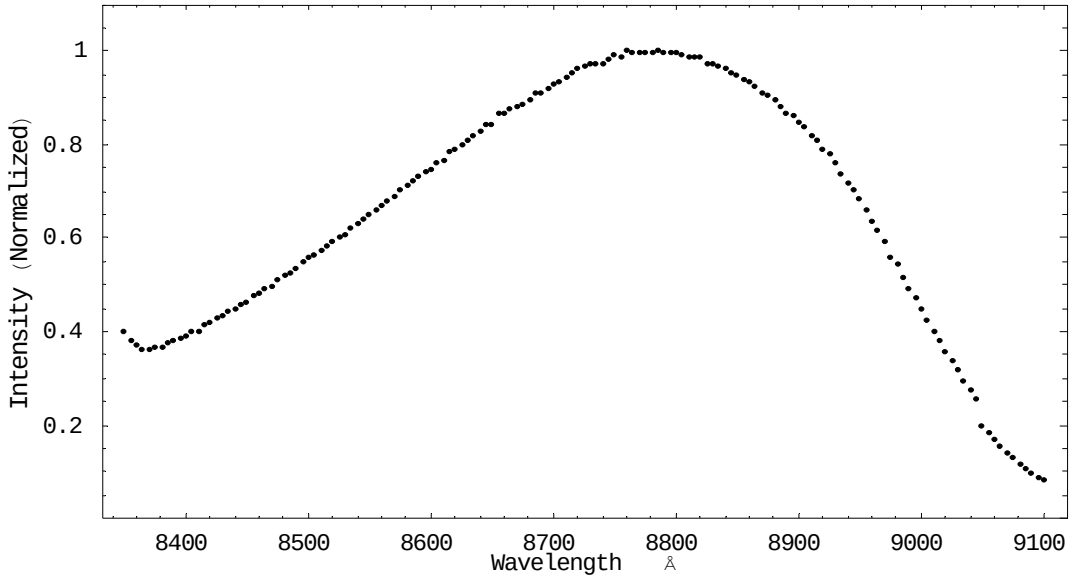

Figure 11. Intensity as a function of wavelength of GaAs illuminated at 415 nanometers

Streak Camera Measurements

The first attempt to obtain temporal data was not very successful. The extraction of data with very low signal strength is hard to achieve with the spectrometer, and from Figure 10 the radiant sensitivity for this streak camera is lower at 830 nanometers,

therefore, having even lower signal strength. Another reason for the low signal strength was the vertical entrance slit width. To increase spectral resolution, the slit width, *w*, must be decreased which decreases signal strength. This can be mathematically represented as

$$\Delta\lambda = \frac{aw}{mf} \qquad [35]$$

where, *a*, is the grating groove spacing, *f*, is the spectrometer focal length, and, *m*, is the order of the principle maxima [4:50]. The groove spacing, *a*, scatters a good portion of the light, therefore, reducing the number of photons entering the streak camera.

Temporal resolution is not dependent on spectral resolution for this experiment. Spectral analysis using the spectrometer was accomplished once to determine the samples band gap. The spectrometer and PMT were removed from the setup and the streak camera was lowered to the table's level along with the laser path. The lowered streak camera minimized the possible degradation in alignment of the streak camera. The laboratory table was suspended on air shocks to minimize vibration and the overhead equipment rack was detached from the laboratory table to prevent possible vibration from equipment such as computer fans. The reduction in vibrations should reduce the amount of jitter in the temporal measurements [12]. The periscope was removed because it was not needed and also contributed to a loss of irradiance in the beams path. The cylindrical lens made of glass was replaced with a CaF_2 lens as explained earlier.

With the new streak camera setup complete and aligned, the time-resolved photoluminescent data could be recorded. Three measurements needed to be recorded first to validate the accuracy of the measured decay rates. The first measurement

recorded was of the temporal time range as a function of excitation pulse at FWHM. The second measurement recorded was of the signal strength of the excitation pulse at FWHM as a function of the slit width for the streak camera. The third measurement recorded was of the lifetime from one of the samples as a function of laser power.

Temporal Resolution for Slit Width and Time Range

Before the temporal measurements can be obtained, the streak camera has to be aligned. With the camera sitting firmly on the table, the camera's slit housing is adjusted vertically to allow maximum throughput of light and is focused onto the photocathode. The slit width is set to 150 microns and the streak camera records the image of the beam pulse as shown in Figure 12.

The streak camera has six different time range settings which affect the amplitude of the voltage sweep. The different time ranges can affect the temporal resolution, because the number of pixels is fixed at 512 on the streak camera, so when the time range is increased, the voltage sweep decreases and accuracy of the resolution lessens. The minimum temporal resolution of the FWHM as reported by manufacturer's test reports and Jost's thesis is 16.93 pixels at time range one [4:58]. The ratio of the minimum temporal resolution and the set number of pixels multiplied by the maximum time range in each setting gives the best temporal resolution for that time range as given in Table 1.

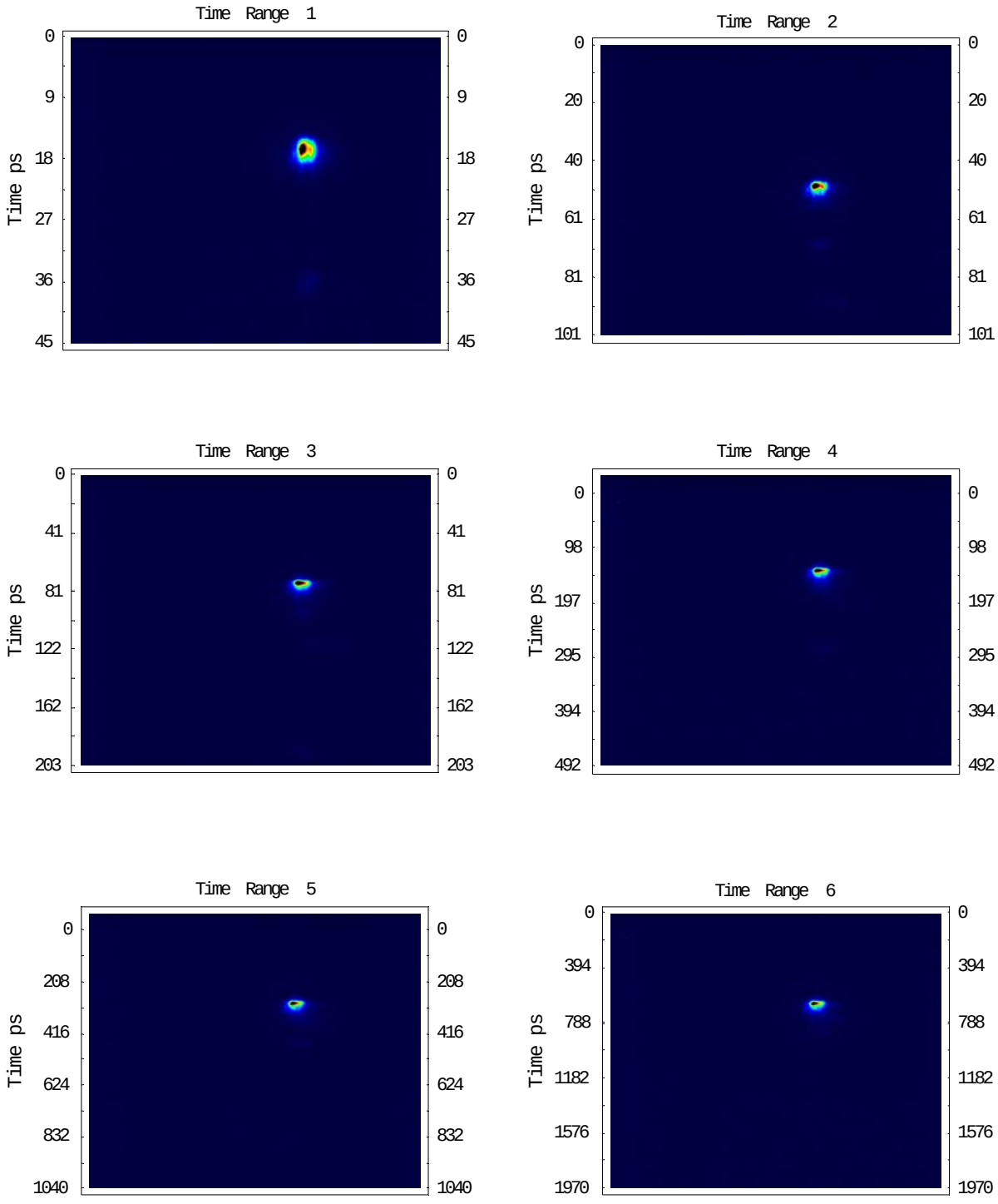

Figure12. Streak image of the excitation pulse at 150 microns slit width for each time range. From left to right, time range one at the top left and time range 6 bottom right

Table 1. Temporal Resolution for each Time Range

Time Range Setting	1
Time Range (ps)	45
Minimum Resolution (ps)	1.49

Each time range has a different minimum temporal resolution for the FWHM of the laser pulse. The FWHM of the laser pulse was obtained for each time range and curve fit using Mathmatica non-linear regression to

$$G = e^{-t^2/2\sigma^2} \qquad [36]$$

where, *G*, is the Gaussian shape for the laser pulse, *t*, represents the temporal variable, and, σ, is the standard deviation of the Gaussian shape. Figure 13 is a plot of the FWHM of the laser pulse as a function of the time range setting. Each plot in each time range represents an average fit of three scanned pulses. The standard deviation, σ_{sd}, is the corrected standard deviation of the FWHM of the laser pulse from the streak camera as shown

$$\sigma_{sd} = \sqrt{\sigma_c^2 + c_t^2} \qquad [37]$$

where, σ_c, is the fit error calculated from Mathmatica non-linear regression routine and, σ_t, is the error of the calibration from the streak camera's temporal range. The calibration adjustment for the streak camera's temporal axes is accomplished by using an etalon that is calibrated to 20 picoseconds. The etalon takes the laser pulse and delays

that pulse by 20 picoseconds. The measurement from the center of gravity of one image, which is represented as a laser pulse peak, to the next image will give the difference in picoseconds. The ratio of 20 picoseconds to the measured difference is calculated and the error is determined.

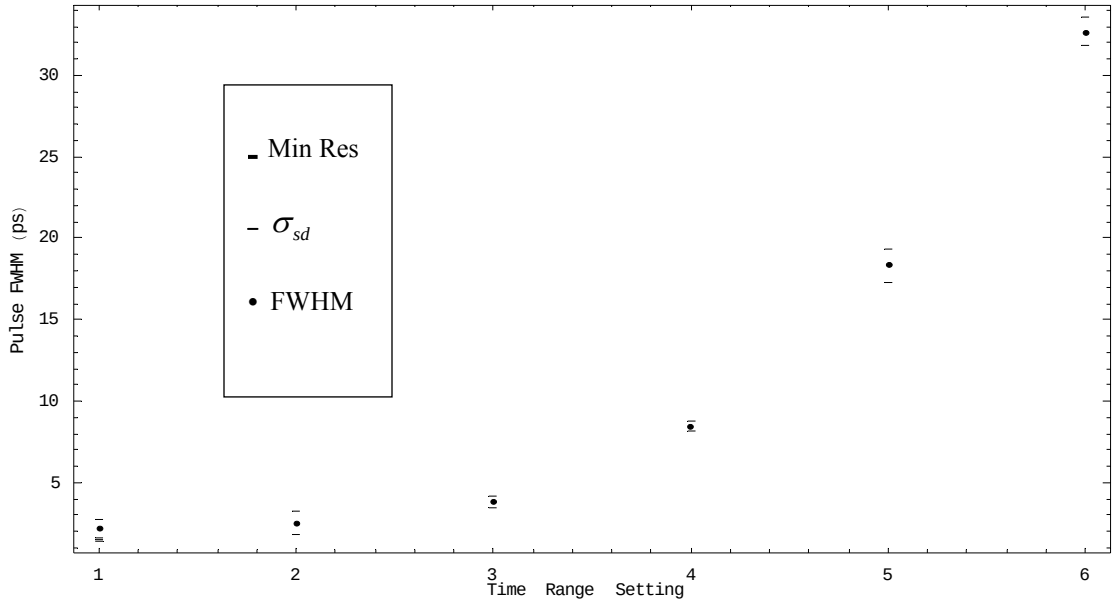

Figure 13. Time range as a function of FWHM of the laser at 150 microns slit width where σ_{sd} is the standard deviation

As explained earlier, the slit width on the spectrometer has an affect on spectral resolution. In the streak camera, the slit width has an affect on temporal resolution. When the slit width on the streak camera narrows, less light enters but resolution increases. In Figure 14, laser pulses were imaged at a slit width ranging from 30 microns to 5 millimeters. Jost had reported that good temporal resolution for the streak camera can be obtained with the slit width less than 50 microns and the best results were at 30 microns. In Figure 14, the best temporal resolution obtained was around 140 to 150 microns and with any narrower slit width, resolution rapidly decreased. After 95 microns, the slits seemed to close as indicated by Figure 14. The only explanation for

this is the micrometer used for adjusting the slit width was out of calibration by 95 microns. The 95 microns is set to 0 microns and the best possible temporal resolution is now at 45 to 65 microns. The only other way to confirm the misalignment is to dismantle the streak camera head and measure the slit width under a microscope.

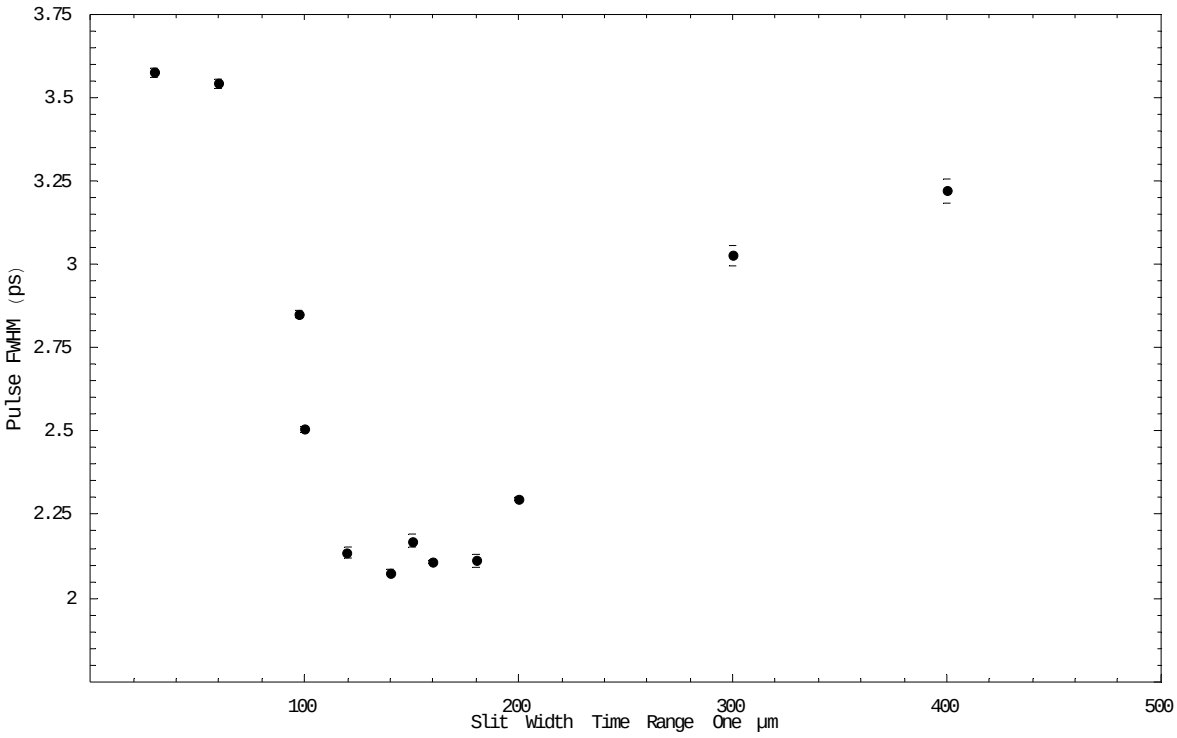

Figure 14. Laser pulse at different slit width; notice the best resolution between slit width 120 and 180 microns or after the adjustment slit width is between 35 and 85 microns.

Temporal Resolution as a Function of Laser Power

Since the slit width and the streak camera time range were shown to have an effect on temporal resolution, the next step was to see if the laser power had an effect on temporal resolution. To accomplish this, one of the samples was excited by the excitation pulse and decay rates were determined. Then, several neutral density (ND) filters were placed in the excitation beam pulse path to reduce the power of the beam on the sample. Three different ND filters with filter ratings at 0.04, 0.1, 0.3, and several combinations of

them, were used to reduce the power. The sample decay rates were calculated for each filter and plotted as shown in Figure 15. There were no significant changes in temporal resolution or the decay rates of the sample at different power levels. Because the carrier lifetime is independent of pump power, radiative recombination and Auger play no significant part in carrier recombination as shown in equation [29]. As power increases, radiative recombination increases as n^2 and Auger increases as n^3. Yet, Figure 15 does not show any change in decay rates, which concludes beyond a doubt that radiative recombination and Auger are insignificant in these samples.

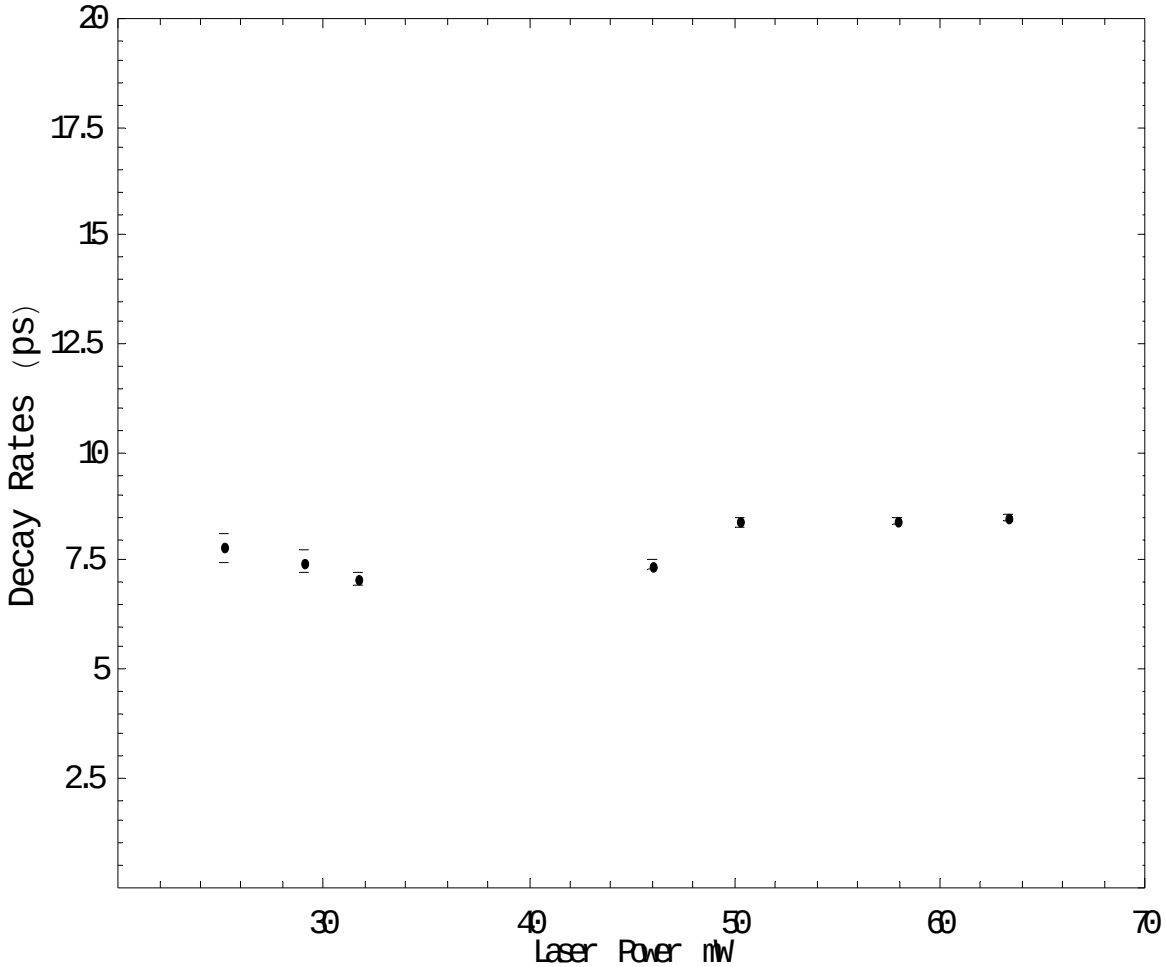

Figure 15. Decay Rates as a function of Laser Power shows that lifetimes are constant for the different power levels.

Experimental Procedures and Setup for Pump Probe Reflectivity

The Time-Resolved Pump Probe Reflectivity (TRPPR) is another technique for studying and finding lifetime in materials. The setup uses the same laser setup as the Time-Resolved Photoluminescence (TRPL) experiment. There are two different laser path lengths used to accomplish this experiment, the 415 nanometers pump beam and the 830 nanometers probe beam. The pump beam leaves the SHG and is aligned through a variable optical delay consisting of a translation stage and a corner cube mirror. The pump beam is then sent through a chopper and a high pass (blue glass: BG-39) filter and focused with a 500 millimeter focal length lens onto the sample. The 830 nanometers probe beam strikes the sample at the same location as the pump beam, albeit with a slightly smaller spot size, because a 250 millimeter focal length lens is used to focus the probe beam. Since the pump light is at a different wavelength from the probe light, a half-wave plate or polarizer was not needed.

In order for the pump and probe pulses to overlap, both beam must have the same optical path length. The zero delay is the point when both pulses arrive at the sample at the same time. It is very important to have the zero delay position determined precisely, or the change in reflectivity will never be found. The alignment of the translation stage should not vary the pump beam when it is translating through its entire length. The translation stage is measured by counts, where 10,000 ± 79 counts equal one millimeter. To convert the translation stage's position in millimeters to time in picoseconds is accomplished by multiplying times two (because the optical path changes twice as fast as the translation stage) and then dividing the distance traveled by the speed of light, thus giving the time axes.

A beam splitter is placed in the probe beam path to redirect some of the beam to an autocorrelator in order to measure the pulse width. The probe beam is reduced in intensity by an ND filter and then focused using a 250 millimeter focal length lens onto the same spot as the pump beam. The reduction in probe intensity is to prevent excitation from the probe's pulse. The ratio of pump photons to probe photons was about 8:1. The probe beam is offset at a different angle of incidence from the pump beam, as shown in Figure 16 and the specularly reflected light from the probe beam is collected by a detector. The detector is a balanced photodiode system designed to reduce background noise produced by the laser. The photodiode converts the light input into an electrical signal which is sent to a lock-in amplifier with the chopper as the reference. The lock-in amplifier measures the change in the light intensity which is converted into an electrical signal from the photodiode due to the change in the index of refraction from the sample's excitation and decay. The change in index of refraction will be discussed next.

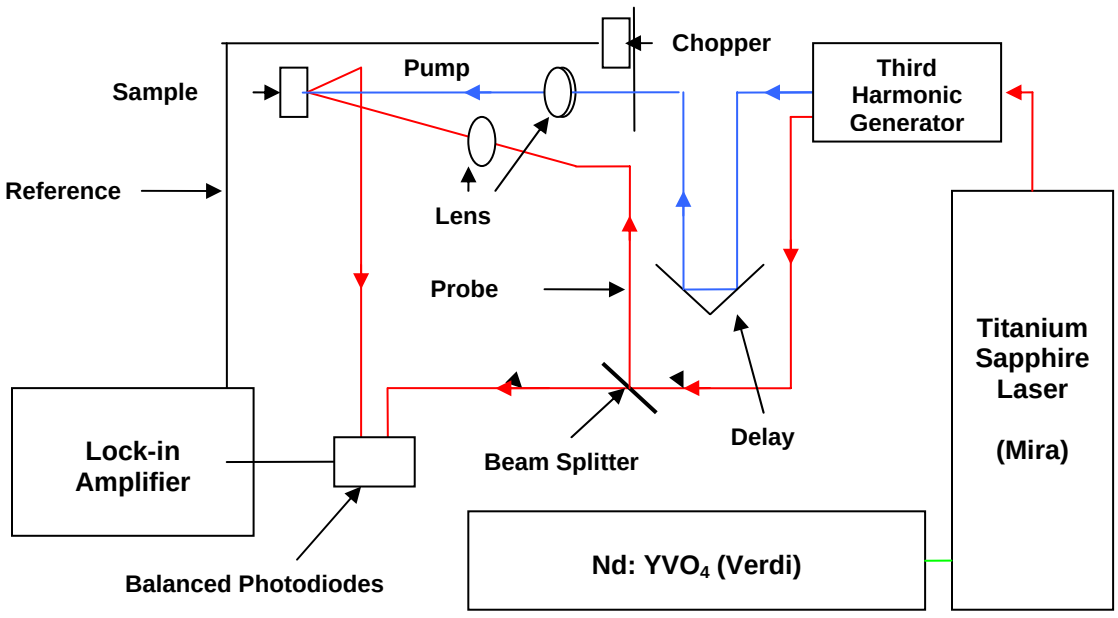

Figure 16. Time Resolved Pump Probe Reflectivity setup.

Change in Index of Refraction

In the TRPPR, the recombination rate of the carriers is determined by the change in reflectivity of the sample. When the semiconductor sample is illuminated by an excitation pulse, electrons are excited into the conduction band; these free carriers change the index of refraction in the sample. As the carriers decay back into the valence band, the index of refraction changes back at a rate following the decay rate and carrier cooling [17:7808]. The probe pulse of the system measures this change in the index of refraction as a precise function of optical delay. The change in reflectivity, by the Drude model, is given as

$$\frac{\Delta R}{R} = \frac{\Delta n}{n^2 - 1} \cdot \frac{\pi e^2}{\varepsilon m_c^*} \cdot \frac{P\lambda^3}{2\hbar\pi^4 c^3 f_r r^2 d} \qquad [38]$$

where n is the index of refraction, ε, is the dielectric constant for GaAs, m_c^*, is the conduction band's effective mass, P, is laser pump power, λ, is the excitation wavelength, f_r, is the pulse repetition rate, r, is the radius of the spot size focused on the sample, and, d, is the absorption length for GaAs [14:2335].

Focal length can have an effect on the $\Delta R/R$; as the spot size becomes smaller in diameter, the absorption depth becomes deeper for a given pump power as shown in Figure 17, because the semiconductor is being pumped to transparency. The plot for Figure 17 comes from

$$d = \frac{3B_r^2 P(1-R)}{8e\hbar cf^2 f_r \pi^{5/2} \lambda \left(\frac{cem_c}{\lambda\hbar}\right)^{3/2}} \qquad [39]$$

where B_r is the beam radius and f is the focal length. If too many carriers are excited into the conduction band, then the Auger non-radiative recombination will dominate causing the change of reflectivity to become non-linear, therefore, resulting in inaccurate decay rates.

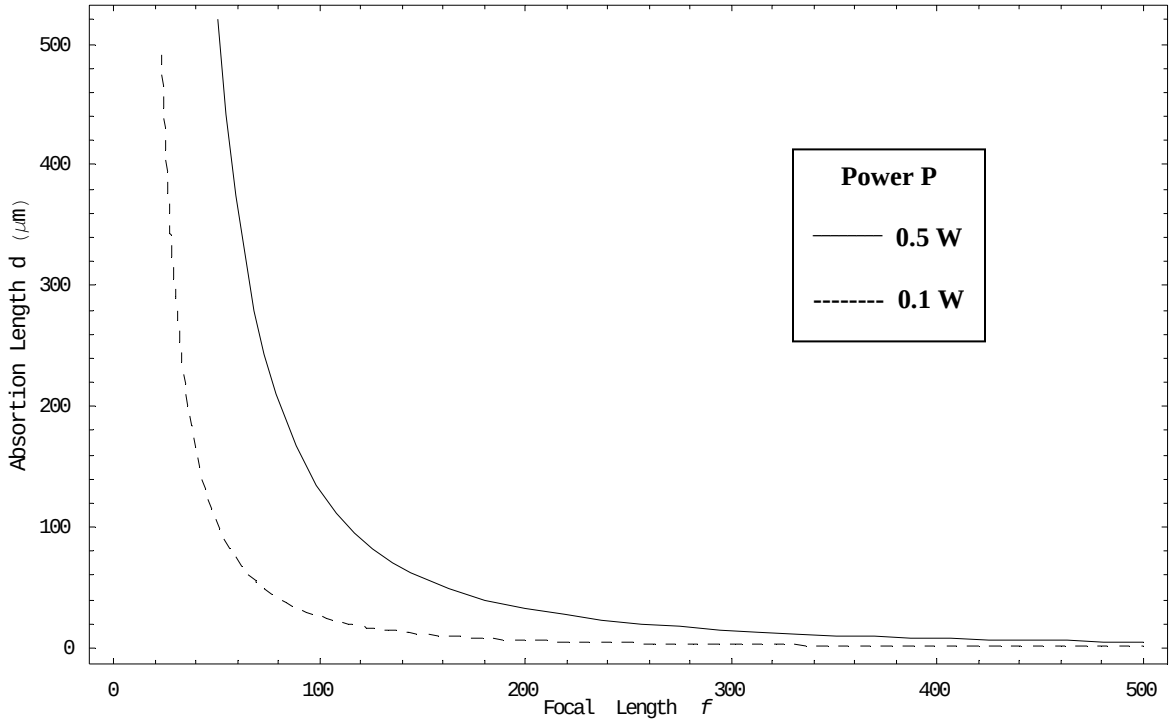

Figure 17. Focal length as a function of absorption depth for various $\Delta R/R$ from equation [39], also pump power effects absorption depths.

IV. Experimental Results

Streak Camera Data and Analysis

The four samples provided by Hanscom AFB were prepared and glued to an aluminum block. Each sample was illuminated by the excitation pulse at room temperature, and the TRPL data was collected by the streak camera. The fluorescence from each of the samples, as detected by the streak camera, is represented in Figure 18. The temporal time scale at time setting one is displayed vertically starting at zero from the top and increasing in time toward the bottom of the page. The decay tail was fit to find the decay rate of the sample. Profile plots of the TRPL from the images are represented in Figure 18, where the intensity is normalized

When the laser pulse is absorbed by the sample as represented by equation [25], many electron-hole pairs are created. Because the photon energy at 415 nanometers is much higher than the band gap energy, the electrons are excited high into the conduction band. The electrons begin to cool very fast back to the conduction band edge, where they begin to bottleneck. The bottleneck at the band edge occurs because the electron's cooling rate to the conduction band edge is much faster than the decay rate back to the valence band. This can be seen in all four plots from Figures 19a and 19b. The initial rise in each plot represents the electrons bunching up at the conduction band edge and starting to decay back to the valence band. When most of the electrons have cooled and more of the electrons at the band edge begin to decay back to the valence band, the intensity of the emitted light reaches a maximum and begins to follow the decay rate for the given sample. The decay plots with the fits are shown in Figures 20a and 20b.

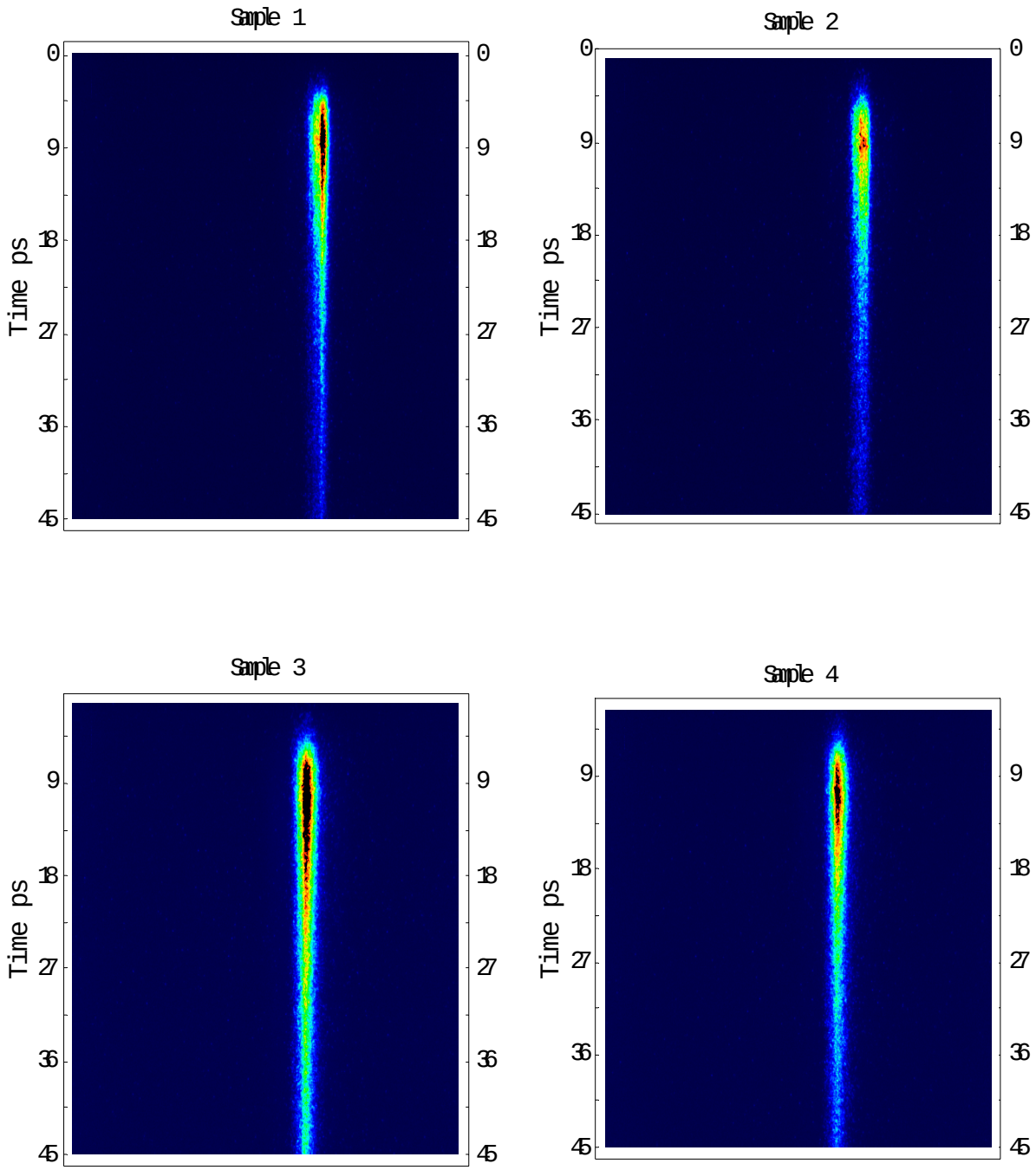

Figure 18. Streak Camera Image for all four samples of GaAs. The horizontal axis represents the horizontal position, and the vertical axis temporal range is 0 to 45 picoseconds (ps).

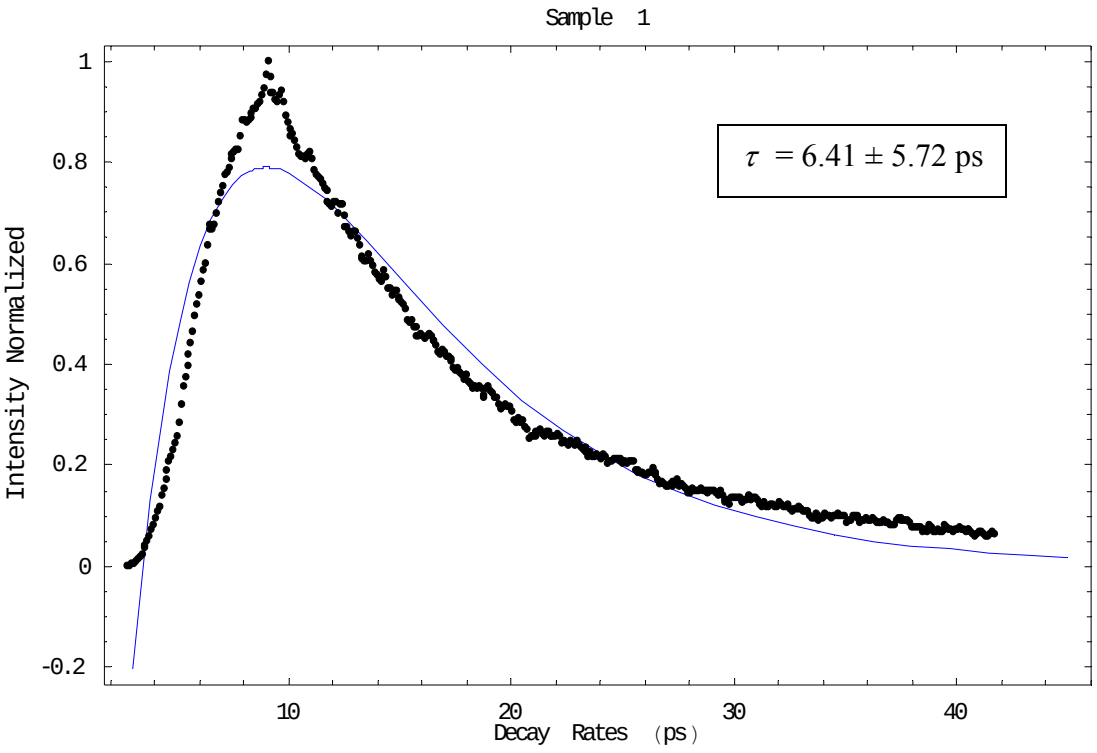

(a)

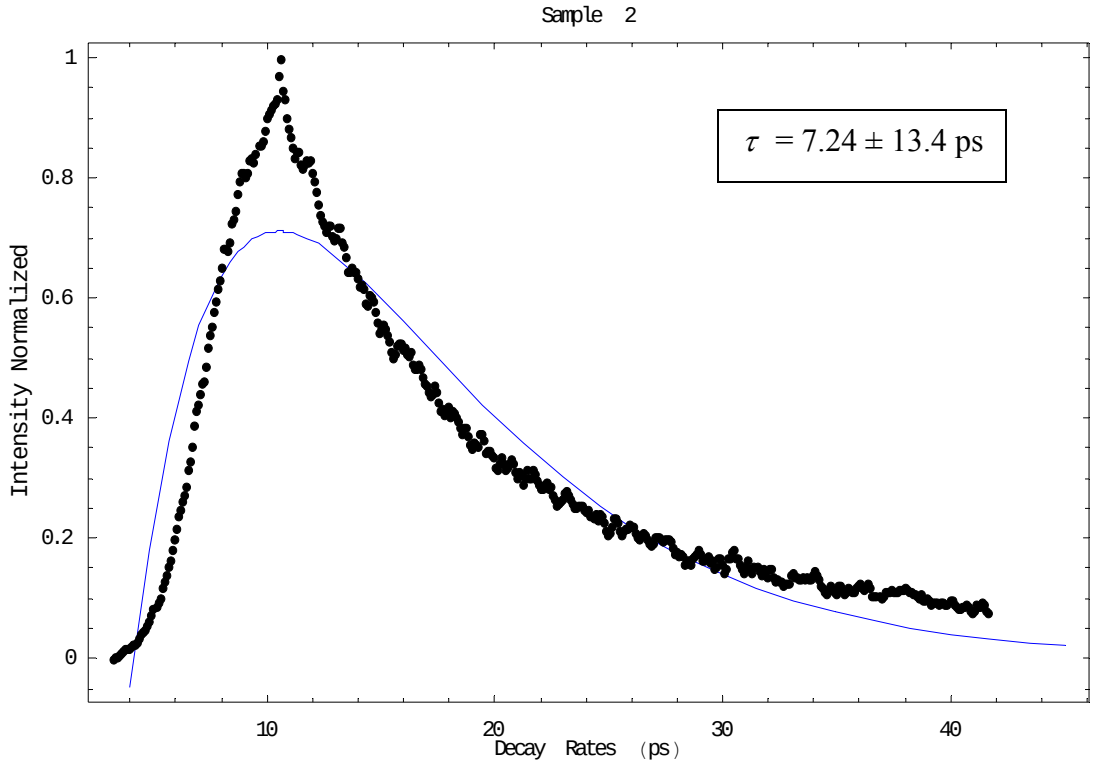

(b)

Figure 19a. Plots of the samples one (a) and two (b) from Figure 18. Each plot, curve fitted using equation [32]

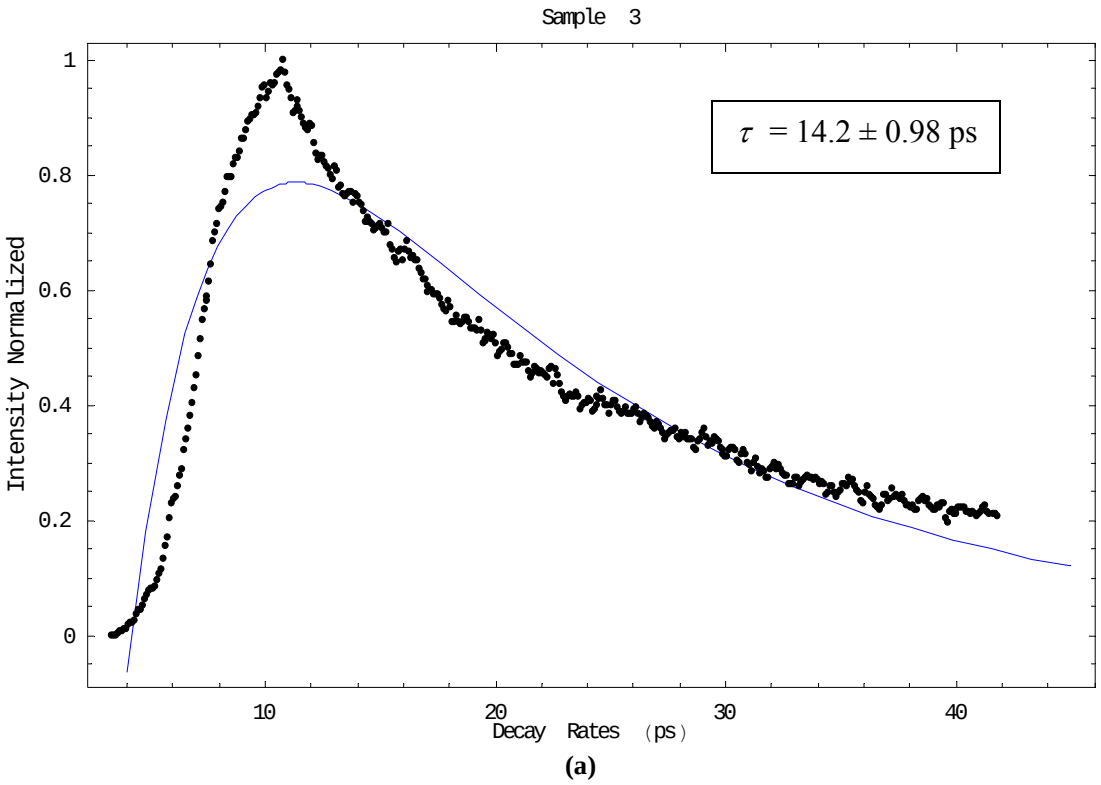

(a)

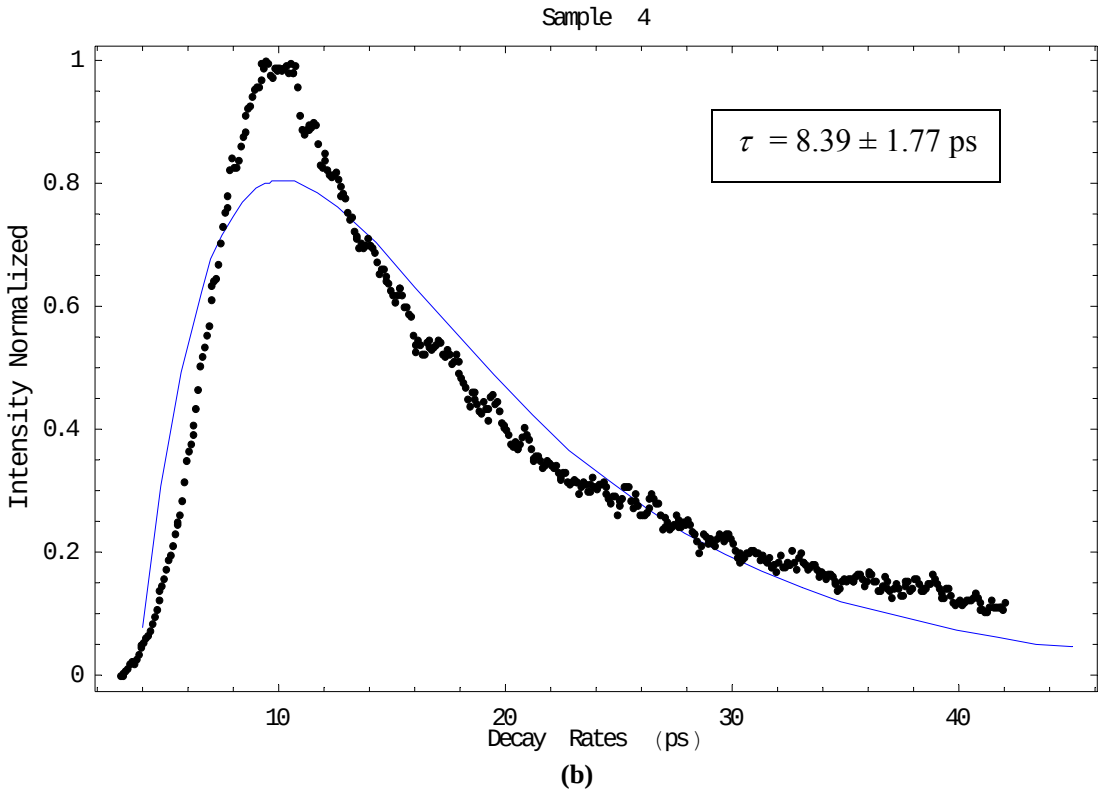

(b)

Figure 19b. Plots of the samples three (a) and four (b) from Figure 18. Each plot, curve fitted using equation [32].

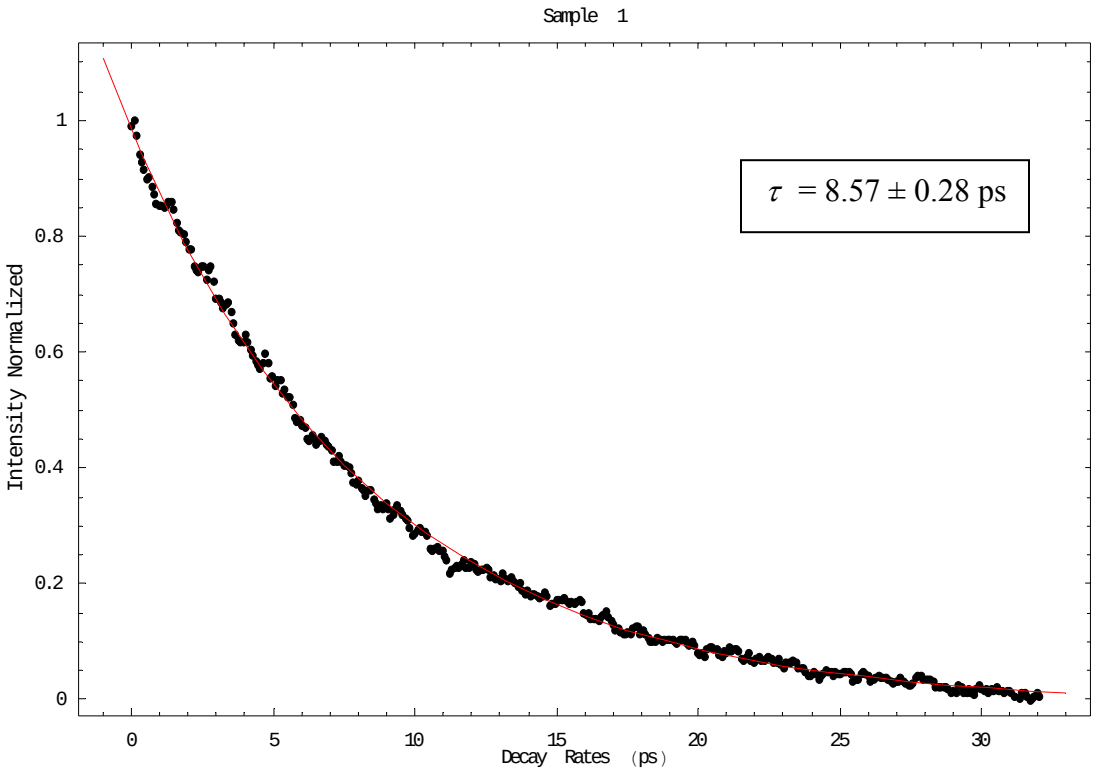

(a)

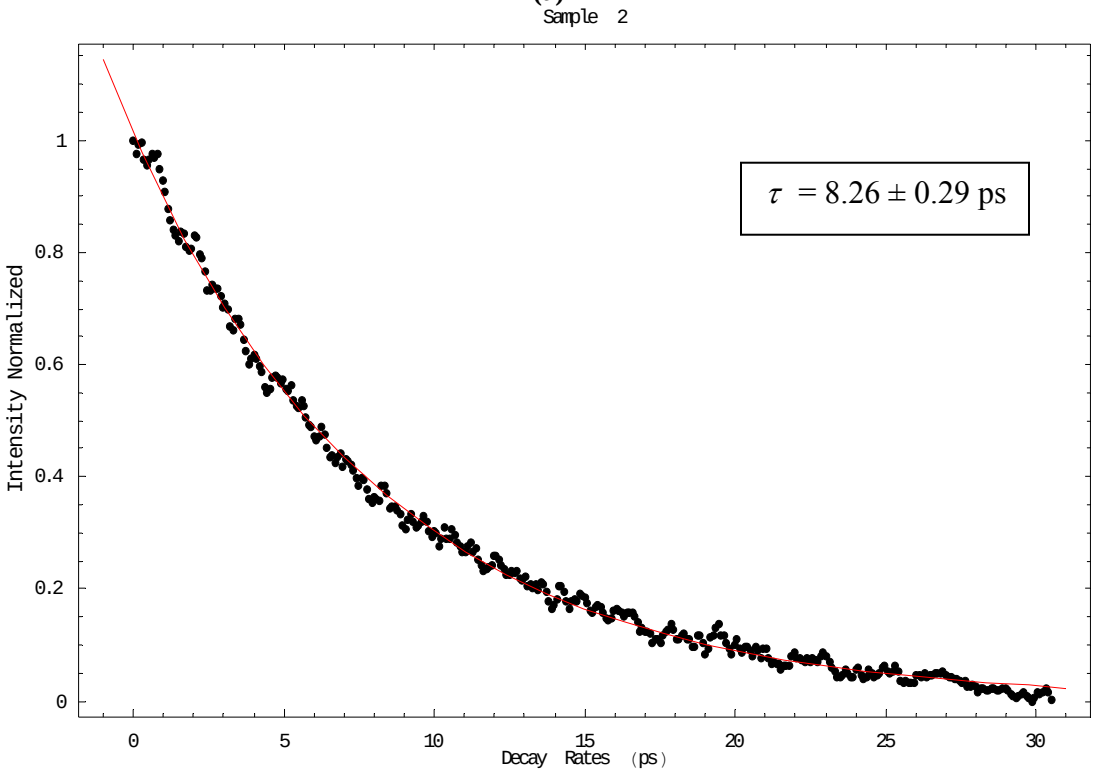

(b)

Figure 20a. Streak camera lifetimes from sample one (a) and sample two (b), linear regression fit of the decay curve and the lifetime for that fit from the natural log of equation [31].

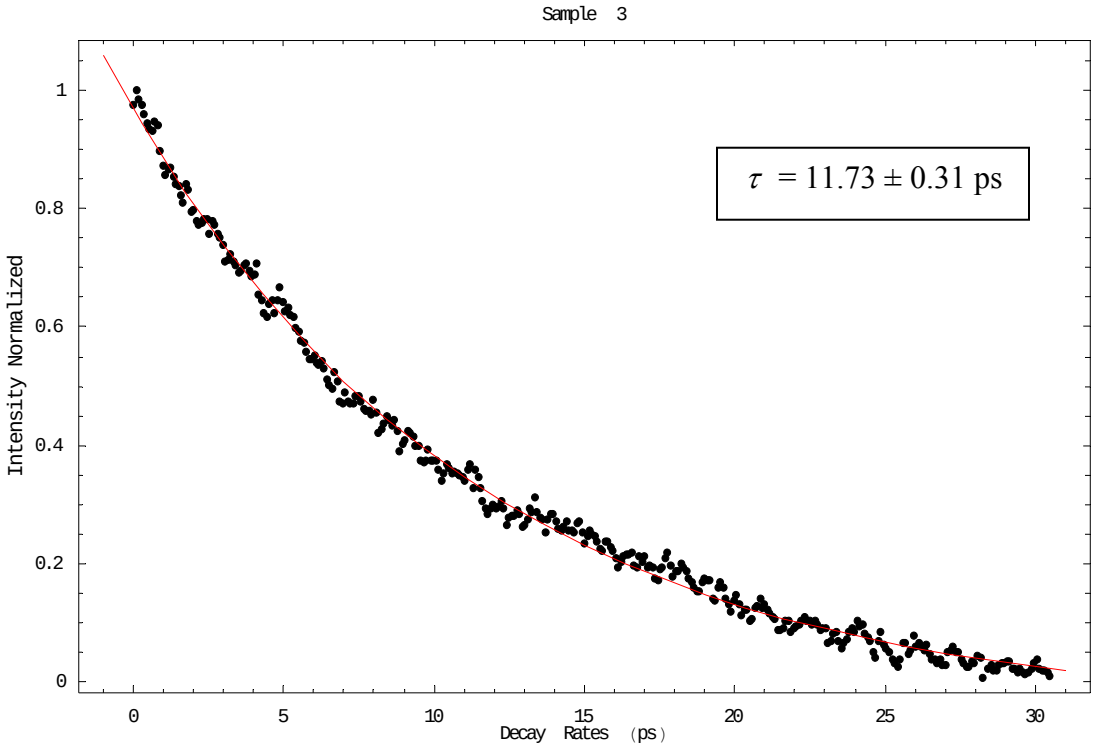

(a)

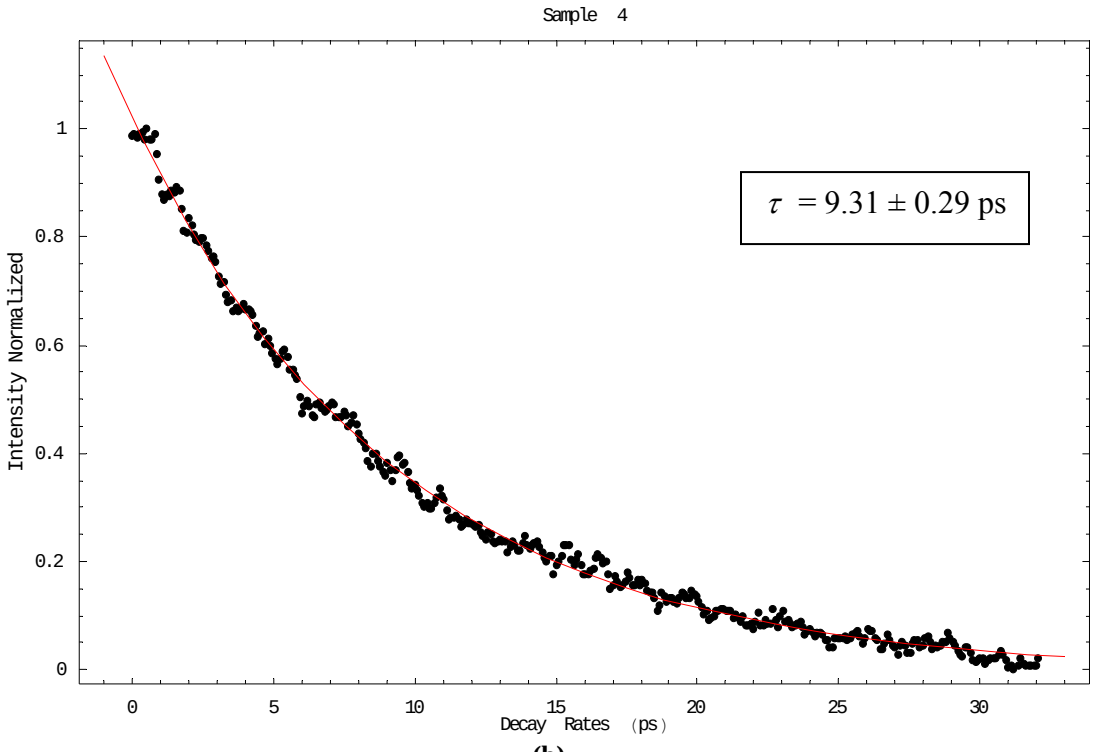

(b)

Figure 20b. Streak camera lifetimes from sample three (a) and sample four (b), linear regression fit of the decay curve and the lifetime for that fit from the natural log of equation [31].

The decay curve was fit using equation [31] and equation [32] for each of the samples as shown in Figures 20a and 20b and Figures 19a and 19b respectively. Linear and non-linear regression using Mathmatica curve fitting was used to find a fit to the data for all four samples. The linear fit was determined by taking the natural log of the data and fitting it. Also, the data from the samples were fit non-linearly using equation [31] and the entire data from Figure 20a and 20b using equation [32] to find the rise and decay of the plot. The process of finding the fits is given in Appendix A. The best fit for the decay curves is from the single exponential and the least square fit; the double exponential fit was good, but the fit was not as precise as shown in Table 2. Using equation [37], the standard deviation for the lifetime of the streak camera was modified. The total standard deviation σ_{sd} is now given as

$$\sigma_{sd} = \sqrt{\sigma_c^2 + a_p^2 + c_t^2} \ . \qquad [40]$$

where, a_p, is the FWHM of the actual pulse. The actual laser pulse width recorded by the autocorrelator multiplied by the 0.684 factor as mentioned previously came out to be 106 femtoseconds. The same calibration adjustment for the streak camera's temporal axis was accomplished as previously mentioned.

The correlation coefficient, R^2, which determines how accurately the data was fit, was calculated at 0.995. The lifetime using the streak camera is given in Table 2. The first two samples have relatively similar lifetime but sample three has a three picoseconds longer lifetime and sample four has a one to two picoseconds longer lifetime because samples three and four were grown with a two order of magnitude difference in

free carrier concentration. The lifetimes are approximately ten times longer than what Hanscom AFB AFRL/SNHC was expecting of 0.5 picoseconds.

Table 2. Decay rates from the streak camera using least square curve fit to equation [31] and [32]

Sample	Lifetime Least square fit	Lifetime Least square fit square root of the data weighted	Lifetime Single exp. Mathmatica nonlinear fit	Lifetime Mathmatica nonlinear fit from Equation [32]
1	8.28 ± 0.28 ps	8.47 ± 0.28 ps	8.57 ± 0.28 ps	6.41 ± 5.72 ps
2	8.04 ± 0.29 ps	8.35 ± 0.28 ps	8.26 ± 0.29 ps	7.24 ± 13.4 ps
3	11.07 ± 0.29 ps	11.27 ± 0.29 ps	11.73 ± 0.31 ps	14.2 ± 0.98 ps
4	9.84 ± 0.29 ps	9.96 ± 0.28 ps	9.31 ± 0.29 ps	8.39 ± 1.77 ps

Experimental Data and Analysis for Pump Probe Reflectivity

The four samples that were used in the streak camera analysis were used in this experiment. The room temperature samples were illuminated and the zero delay point was found. The zero delay point should not change for each sample, but each sample might be sitting differently on the block. The cement used was rubber glue which should not change the properties of the experiment. To insure the cement did not affect the samples, a small amount was used on the top corner and the laser illuminated the bottom section of the sample. Once the sample and optical path of the pump and probe were aligned, data collection began. Each sample was scanned several times to obtain a good

average of the change in reflectivity. The scan began before the zero delay and continued until the decay stopped, usually no longer than three millimeters. The scan rate was run at 5 microns per second to ensure a high resolution.

Figures 21a, 21b and 21c show the plot of the average data obtained for each sample. The samples should decay back to their initial, *R*, value as shown in samples 2 and 4. In samples 1 and 3, the final decay curve is much lower than the initial start. The reason for this is unknown and continued after the scan stopped for a long period of time which would not stabilize. This would cause the final results of the decay rates in both samples to be suspect, but the true decay rates can be determined by subtracting the background drop in, *R*.

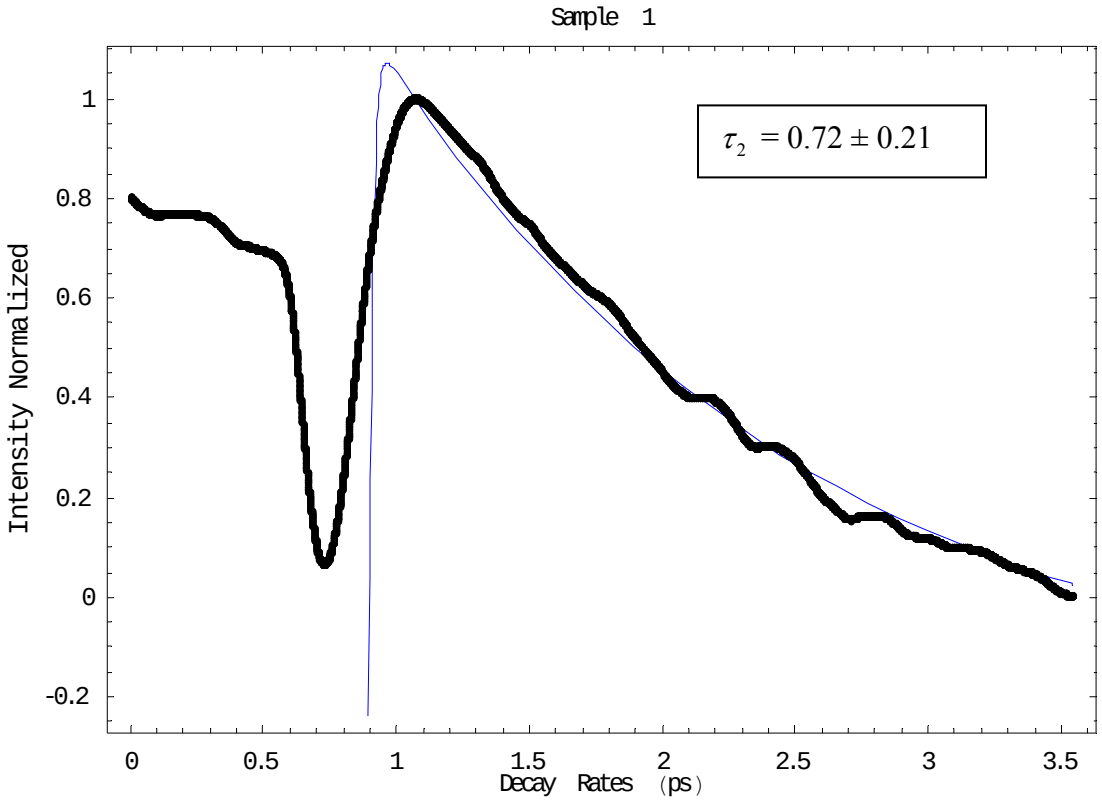

Figure 21a. Pump probe data plots for sample one with the double exponential curve fit and the lifetime from that fit from equation [32]. This plot shows the continued decrease in intensity as compared to Figure 21b (a). Initial drop represents the FWHM of the laser pulse.

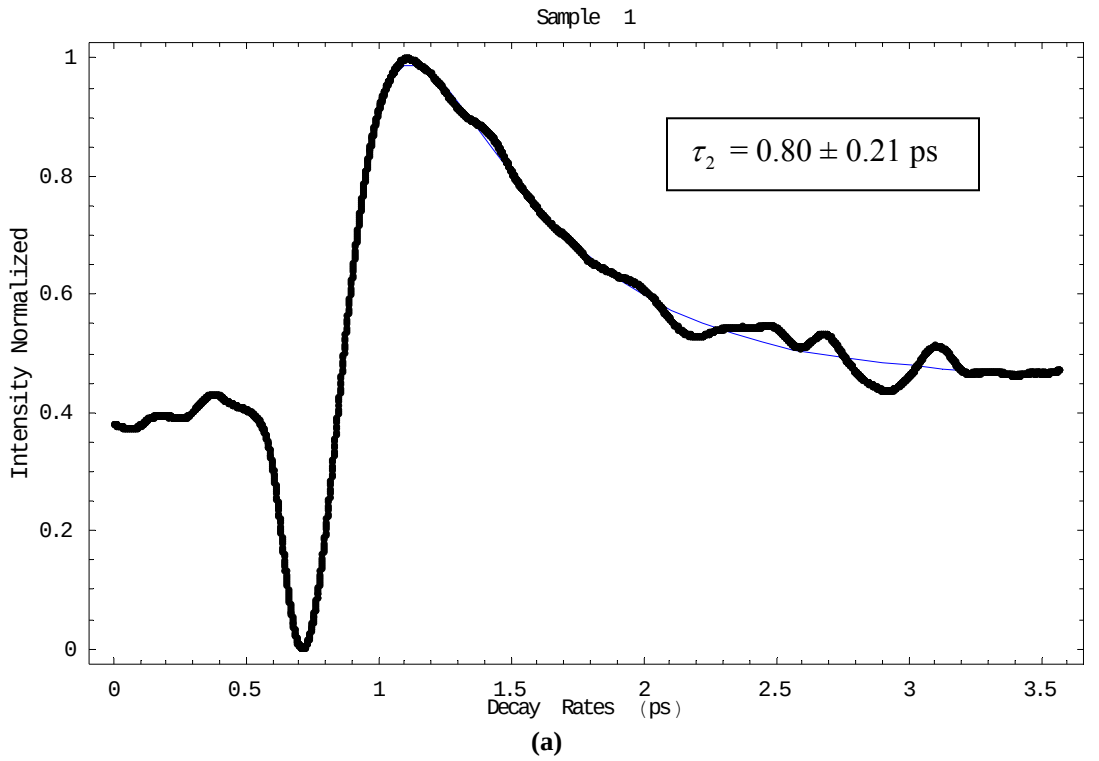

(a)

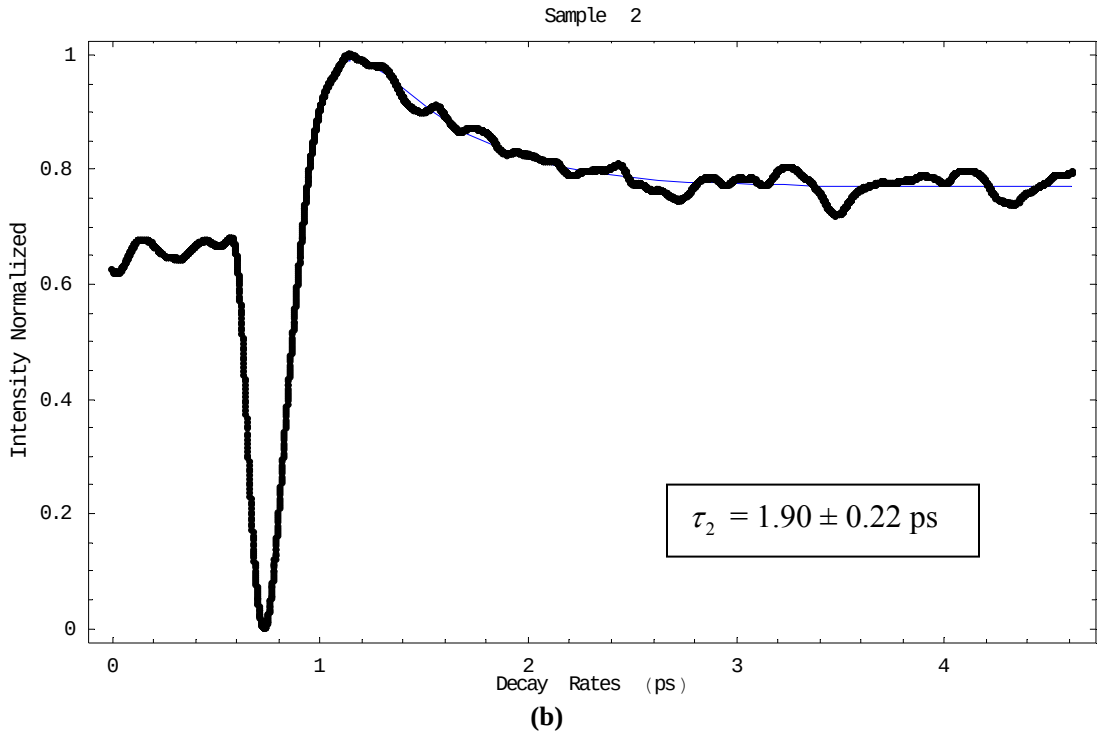

(b)

Figure 21b. Pump probe data plots for sample one (a) (second set) and two (b) with the double exponential curve fit and the lifetimes from that fit from equation [32]. Initial dip in both plots represents the FWHM of the laser pulse.

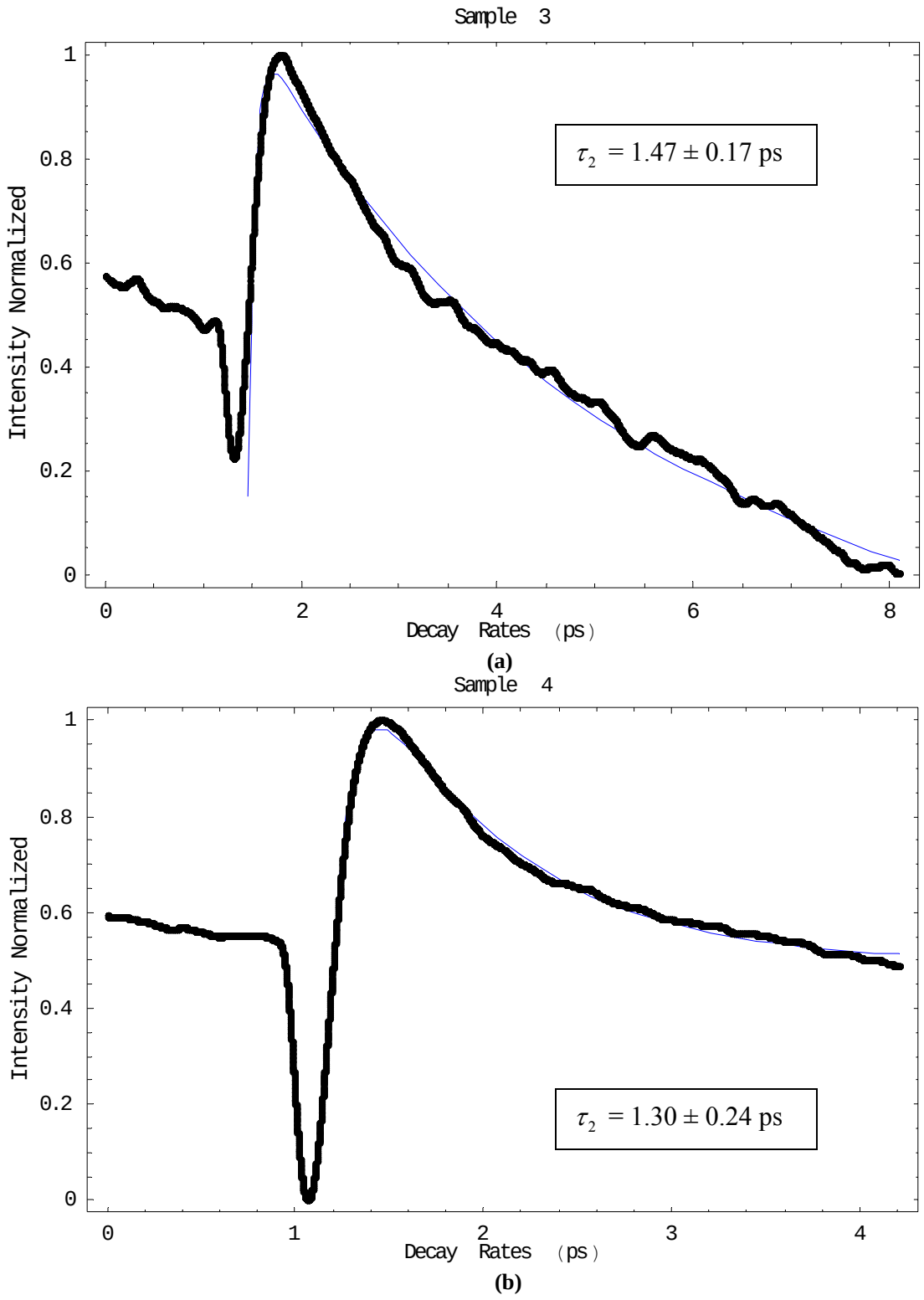

Figure 21c. Pump probe data plots for sample three (a) and four (b) with the double exponential curve fit from equation [32] and the lifetimes from that fit. Plot (a) shows the continued decrease in intensity. Initial dip in both plots represents the FWHM of the laser pulse.

The initial drop in ΔR represents both pump laser beam pulse and the probe laser beam pulse at the time delay zero. This process is the result of the pump laser beam, which is polarized in one direction, exciting the sample, therefore, creating electron-hole pairs. As the polarized pump laser pulse excites the electrons into the conduction band, it creates an electron-hole dipole moment in the direction of the polarized light. The electron-hole dipole moment becomes random, after the, τ_2, dephasing time. This predominately non-radiative recombination rate is the decay curve. The initial drop in each plot represents the autocorrelation of the FWHM of the laser pulse; therefore, the FWHM of the laser pulse should match the FWHM of the dip in each plot. Each plot from Figure 21a, 21b and 21c had to be corrected on the temporal axes to match the actual FWHM of the laser pulse. The reason for this discrepancy is unknown, but might be the result of the integration time selected chosen on the lock-in amplifier.

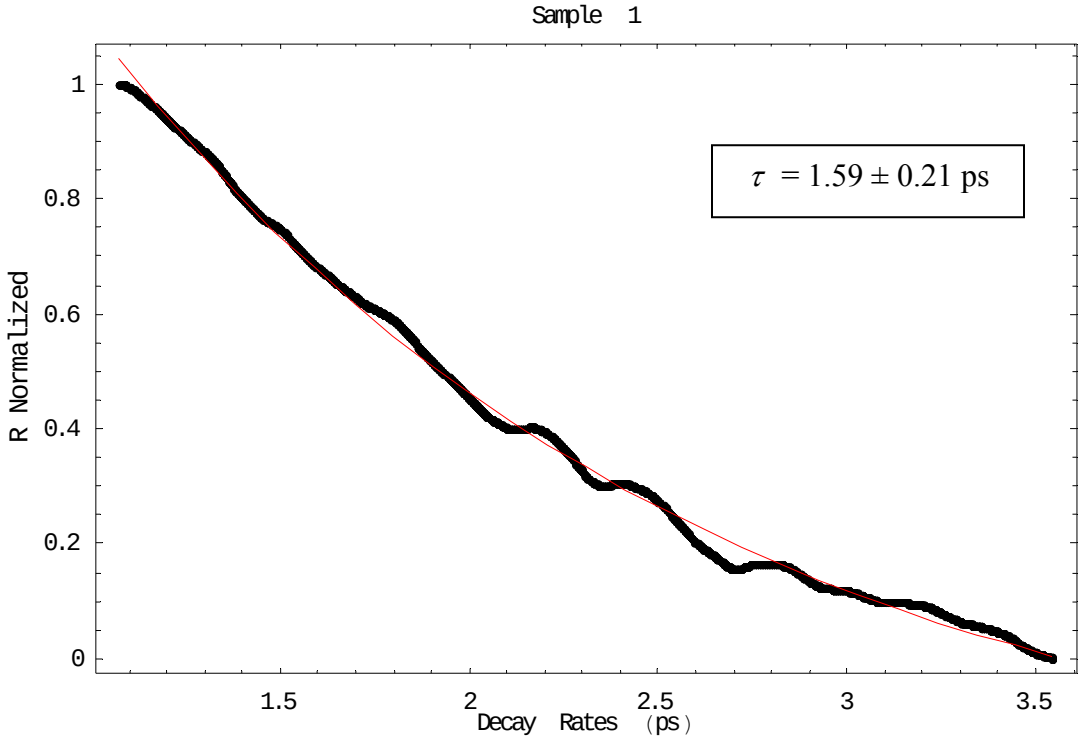

Figure 22a. Pump probe data plots for sample one and fitted exponential curve.

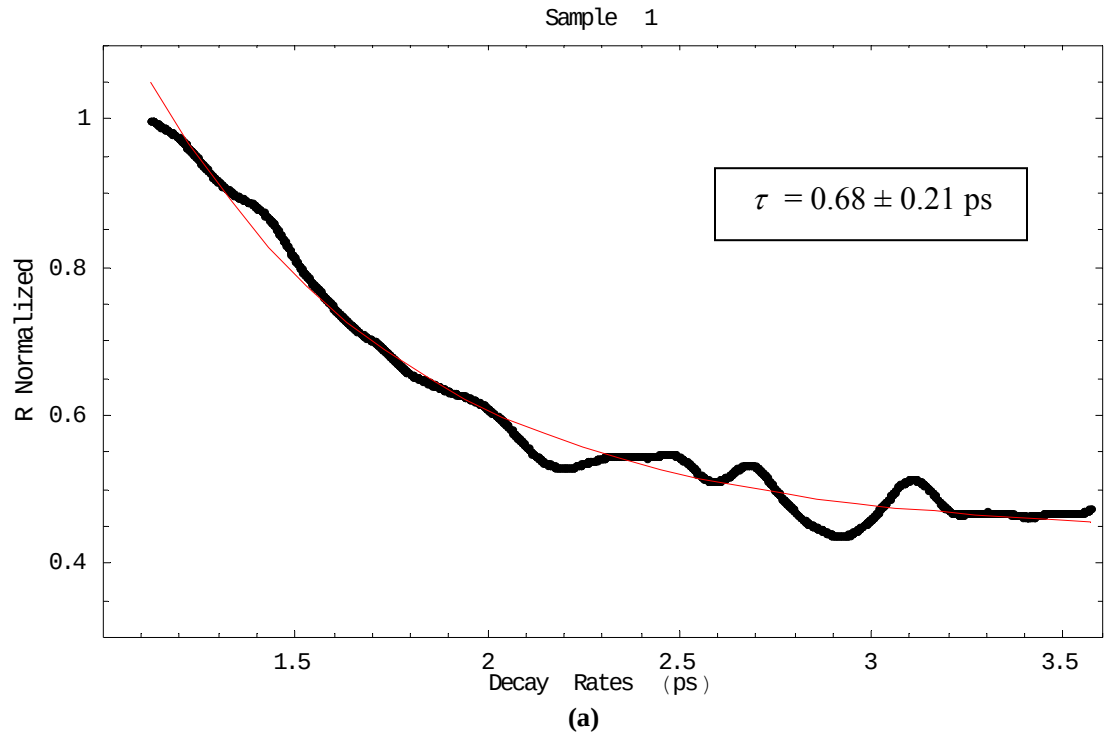

(a)

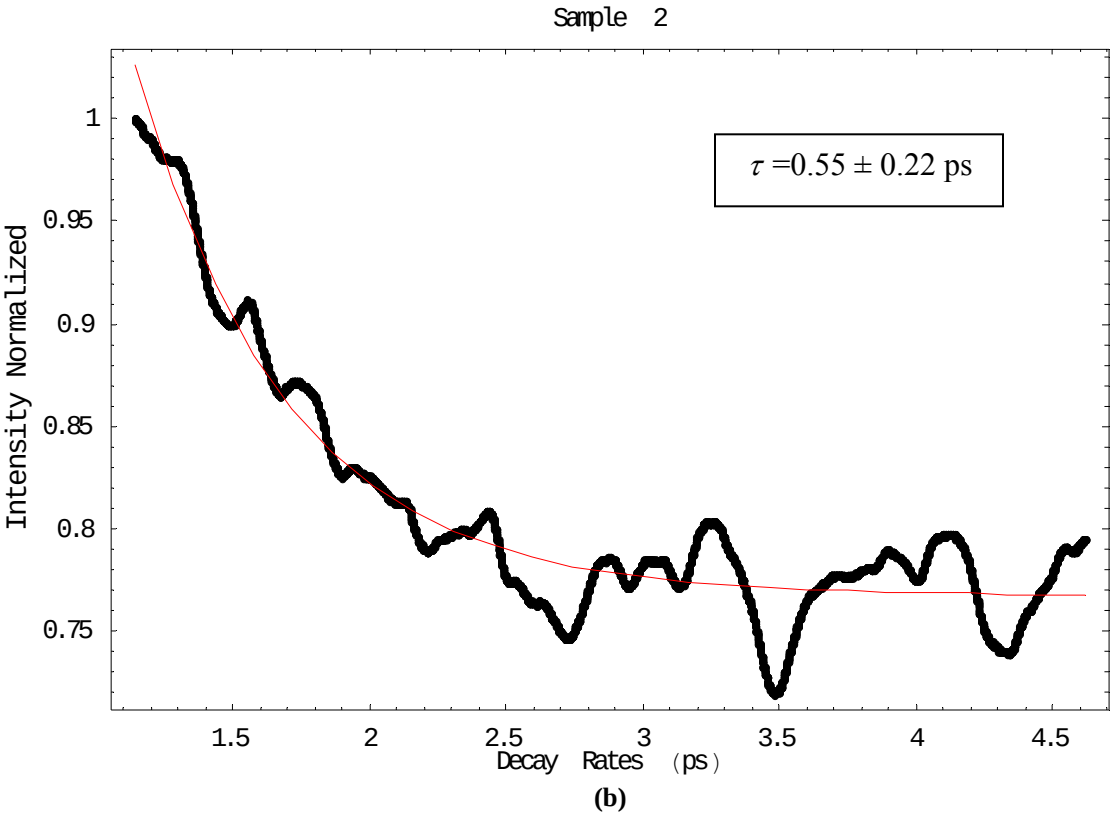

(b)

Figure 22b. Pump probe data plots for sample one (second set of data taken) (a) and two (b) and fitted exponential curve.

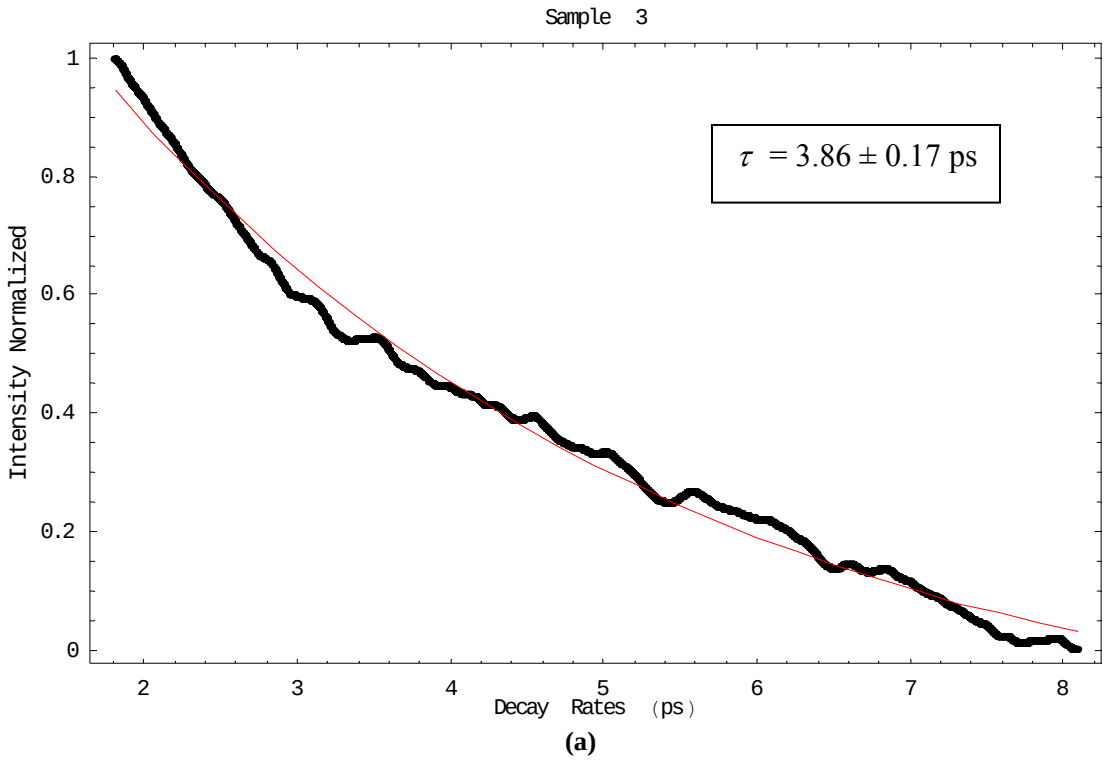

(a)

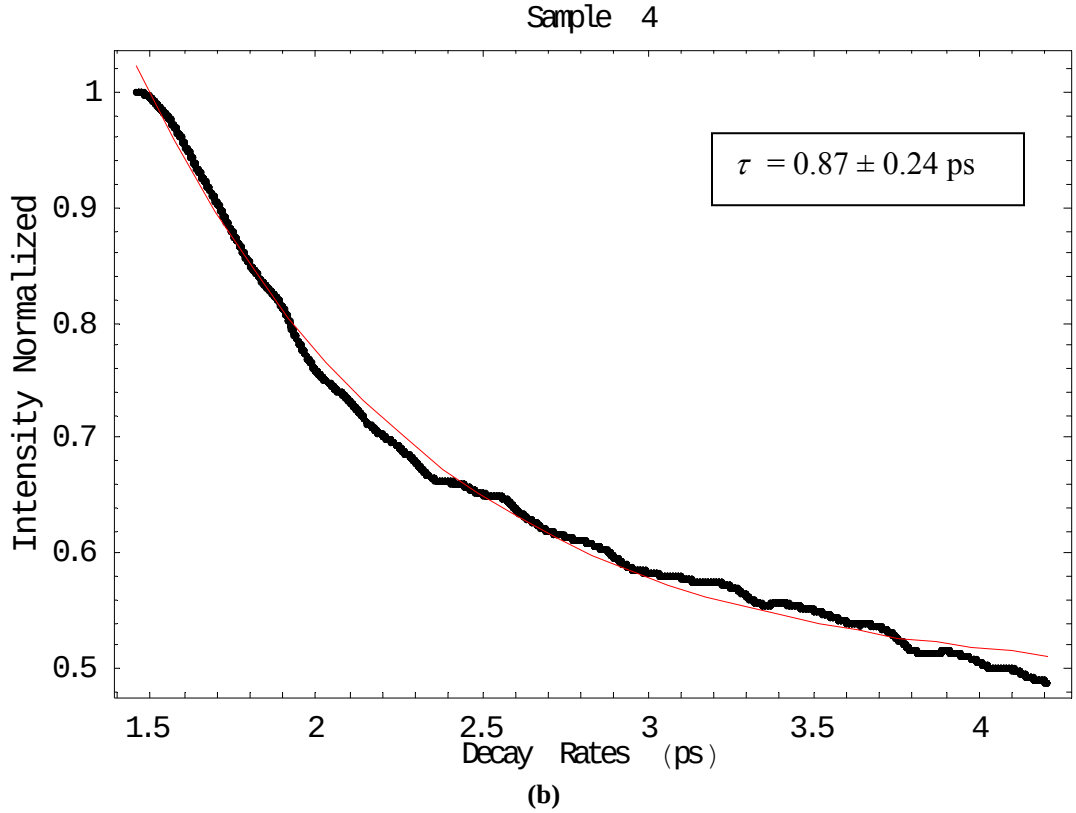

(b)

Figure 22c. Pump probe data plots for sample three (a) and four (b) and fitted exponential curve.

Again, the four samples' decay curves were fit as shown in Figures 22a, 22b, and 22c and their decay rates were determined. Each fit was calculated by taking the natural log of the decay curve and using linear regression to determine the decay rate. The data from all four samples were also fit non-linearly using equation [31] to find the best single and the best double exponential fit. Figures 22a, 22b, and 22c represent the curve fit using linear regression with the data weighted. The, R^2, was calculated to be between 0.9 and 0.95. The final lifetimes from all different fits for the pump-probe technique are given in Table 3.

Table 3. Decay Rates from Pump Probe Reflectivity data using Linear Regression Curve Fitting to Equation [31] and [32]

Sample	Lifetime Least square fit	Lifetime Least square fit of the weighted data square rooted	Lifetime Single exp. Mathmatica nonlinear fit	Lifetime Mathmatica nonlinear fit from Equation [32]
1	1.60 ± 0.21 ps	1.60 ± 0.21 ps	1.59 ± 0.21ps	0.72 ± 0.21 ps
1	0.76 ± 0.21 ps	0.77 ± 0.21ps	0.68 ± 0.21 ps	0.80 ± 0.21 ps
2	2.26 ± 0.22 ps	2.09 ± 0.22 ps	0.55 ± 0.22 ps	1.90 ± 0.22 ps
3	3.78 ± 0.17 ps	3.83 ± 0.17 ps	3.86 ± 0.17 ps	1.47 ± 0.17 ps
4	1.32 ± 0.24 ps	1.30 ± 0.24 ps	0.87 ± 0.24 ps	1.30 ± 0.24 ps

The fitting was harder to obtain because of the oscillations in the data. All samples have relatively similar lifetime compared to each other but have lifetime faster

than the streak camera's lifetime. The explanation for the faster lifetimes is that in the TRPPR technique there are more effects than just carrier decay. One effect is the band gap renormalization (BGR) and the band filling (BF), where the carriers that are excited high into the conduction band, changes the band gap itself. The decay of the carriers represents two different decays, one being the decay due to carrier cooling and the other due to carriers decaying back to the valance band [17:7807].

V. Conclusion and Recommendation

Conclusions of Research

The analysis of GaAs samples supplied from the AFRL/SNHC at Hanscom AFB is complete. The results from both experiments can be compared for each sample. The results of the fit from the decay curves of the streak camera range from 8.3 ± 0.3 picoseconds to 11 ± 0.3 picoseconds depending on the sample. The results of the fit from the decay curves of the TRPPR range from 0.8 ± 0.2 picoseconds to 3.8 ± 0.2 picoseconds. The carrier lifetime from the samples of the streak camera could generate terahertz radiation in the range of 0.12 THz to 0.09 THz, whereas the carrier lifetime from the TRPPR would generate terahertz in the range of 1.3 THz to 0.3 THz. The streak camera results fall short by a factor of ten from the desired terahertz generation range of 1 THz to 5 THz, except for the TRPPR the lifetime come within the desired results. The GaAs growth technique needs to be changed to increase the carrier lifetime, perhaps by increasing the dopins in future GaAs samples.

The lifetimes from the TRPPR are almost ten times faster than the lifetime from the streak camera. As explained earlier, the reason for these faster lifetimes is carrier cooling and carrier decay where they are both present in the decay curve. Many pump probe experiments have been performed and the change in reflectivity is reported as the carrier lifetime, but Prabhu and Vengurlekar in their article, *Dynamics of the Pump-Probe Reflectivity Spectra in GaAs and GaN* [17], report that there are more variables to consider. Some of these variables to consider are the band gap renormalization, band filling, carrier cooling, and the power levels of the laser pump, which can alter the carrier

lifetime from the true results. This could account for the different lifetime in the TRPPR experiment.

Recommendations for Future Research

With the TRPPR lifetime different than the streak camera's lifetime due to added variables in the TRPPR, an experiment could be implemented to find the effects of the band gap renormalization, band filling, and carrier cooling. The streak camera and the TRPPR could be used together to find the carrier cooling for different GaAs or GaN samples with different lifetimes. An experiment could be devised to find and explain the physics behind band gap renormalization and band filling.

As stated earlier, the coefficient for Auger should be negligible due to the high number of defects in the lattice structure. The Shockley-Read-Hall coefficient will be many orders higher in the carrier lifetime rates due to these high defects. This is the reason why the carrier lifetimes are so short. The TRPL and the TRPPR should be accomplished to confirm that Auger does not have an effect on the carrier lifetime by recording the decay rates at different temperatures. It would be another confirmation that Auger is not a factor in the carrier lifetime and should have the same results, independent of temperature.

The reason both experiments were done was to determine if the carrier lifetime is needed to assess the suitability of these unique thick layers for photo-mixing and ultra-short current pulse generation, and to characterize them for terahertz applications. If the carrier lifetime is short enough and the resistivity is high enough, then terahertz radiation can be generated. One method is to illuminate a GaAs photoconductive switch attached

to an antenna with two cw laser beams that mix in this non-linear material with large second order susceptibility. The difference from both wavelengths is a terahertz, and then radiation at a terahertz frequency should be generated from the photoconductive switch through the antenna. An experiment could be performed to determine if any terahertz frequency is generated.

The TRPPR was very difficult to setup and align, and alignment was the crucial part of the experiment. The pump beam could not drift when the time delay stage translated through its entire range. If the beams misalign, then at zero time delay, the reference beam would not be able to detect the change in the index of refraction. The background noise due to the laser can cause fluctuations in the data, therefore, obtaining a good curve fit can be challenging. Instead of using a translation stage with a corner cube, an alternative setup can achieve better results. The alternative setup consists of a corner cube attached to an oscillating apparatus, such as a speaker, instead of using a translation stage. The oscillation distance would be measured and converted to a time axis and the photodiode would be linked to an oscilloscope. This type of setup would allow for easier alignment, any fluctuations in the laser would be minimized and results would be more accurate.

Appendix A: Mathmatica Curve Fitting Program

This curve fit program in Mathmatica was used on the streak data.

Loading the built in programs to do the curve fitting.

```
<<Statistics`LinearRegression`
<<Statistics`NonlinearFit`
<<Graphics`Legend`
<<Graphics`MultipleListPlot`
```

Importing five streak camera data runs at 150 um slit width.

```
data01=ReadList["F:\Thesis\Lifetimes\dataactual\s1-150um-tr1-
01.txt",{Number,Number}];
data02=ReadList["F:\Thesis\Lifetimes\dataactual\s1-150um-tr1-
02.txt",{Number,Number}];
data03=ReadList["F:\Thesis\Lifetimes\dataactual\s1-150um-tr1-
03.txt",{Number,Number}];
data04=ReadList["F:\Thesis\Lifetimes\dataactual\s1-150um-tr1-
04.txt",{Number,Number}];
data05=ReadList["F:\Thesis\Lifetimes\dataactual\s1-150um-tr1-
05.txt",{Number,Number}];
```

Showing the individual plots of the five streak camera data runs at 150 um slit width.

```
plot1=ListPlot[data01,PlotStyle->RGBColor[1,0,0]]
plot2=ListPlot[data02,PlotStyle->RGBColor[0,1,0]]
plot3=ListPlot[data03,PlotStyle->RGBColor[0,0,1]]
plot4=ListPlot[data04,PlotStyle->RGBColor[1,1,0]]
plot5=ListPlot[data05,PlotStyle->RGBColor[1,0,1]]
```

All five streak camera plots together.

```
Show[plot1,plot2,plot3,plot4,plot5]
```

Finding the maximum's position for each plot.

```
max01=First[First[Position[data01,Max[data01]]]]
max02=First[First[Position[data02,Max[data02]]]]
max03=First[First[Position[data03,Max[data03]]]]
max04=First[First[Position[data04,Max[data04]]]]
max05=First[First[Position[data05,Max[data05]]]]
```

Finding the time from the maximum.

```
pos01=data01[[max01,1]]
pos02=data02[[max02,1]]
pos03=data03[[max03,1]]
pos04=data04[[max04,1]]
pos05=data05[[max05,1]]
```

Aligning the plots to each others maximum.

```
data02[[All,1]]=data02[[All,1]]+(pos01-pos02);
data03[[All,1]]=data03[[All,1]]+(pos01-pos03);
data04[[All,1]]=data04[[All,1]]-(pos04-pos01);
data05[[All,1]]=data05[[All,1]]+(pos01-pos05);
```

Finding the number of data points taken so the five runs can be averaged.

```
Position[data01,Last[data01]]
Position[data02,Last[data02]]
Position[data03,Last[data03]]
Position[data04,Last[data04]]
Position[data05,Last[data05]]
```

Finding the maximum of the data so the five runs can be matched up at their peaks.

```
Position[data01,Max[data01]]
Position[data02,Max[data02]]
Position[data03,Max[data03]]
Position[data04,Max[data04]]
Position[data05,Max[data05]]
```

Editing the data so the lengths will be equal, therefore, allowing Mathmatica to run the data.

```
data01=Drop[data01,{1,13}];
data02=Drop[data02,{1,23}];
data03=Drop[data03,{1,9}];
data04=Drop[data04,{1,20}];
data01=Drop[data01,{-21,-1}];
data02=Drop[data02,{-8,-1}];
data03=Drop[data03,{-9,-1}];
data05=Drop[data05,{-14,-1}];
```

Verifying the data lengths are equal and the maximums are at the same time.

```
Position[data01,Last[data01]]
Position[data02,Last[data02]]
```

```
Position[data03,Last[data03]]
Position[data04,Last[data04]]
Position[data05,Last[data05]]
```

Verifying the data lengths are equal and the maximums are at the same time.

```
Position[data01,Max[data01]]
Position[data02,Max[data02]]
Position[data03,Max[data03]]
Position[data04,Max[data04]]
Position[data05,Max[data05]]
```

Verifying the plots are aligned to each other.

```
plot11=ListPlot[data01,PlotStyle->RGBColor[1,0,0]]
plot22=ListPlot[data02,PlotStyle->RGBColor[0,1,0]]
plot33=ListPlot[data03,PlotStyle->RGBColor[0,0,1]]
plot44=ListPlot[data04,PlotStyle->RGBColor[1,1,0]]
plot55=ListPlot[data05,PlotStyle->RGBColor[1,0,1]]

Show[plot11,plot22,plot33,plot44,plot55]
```

Averaging of all five data plots.

```
data=data01;
data[[All,2]]=(data01[[All,2]]+data02[[All,2]]+data03[[All,2]]+data04[[All,2]]+data05[[
All,2]])/5;
```

Finding the maximum in the plot to cut off the initial increase, so the decay part of the curve can be determined.

```
data02=data[[All,2]];
position01=First[First[Position[data02,Max[data02]]]]+5;
data03=Drop[data,{1,position01}];
```

Finding the minimum to normalize the decay curve.

```
data04=data03;
min01=Min[data03[[All,2]]];
data03[[All,2]]=data03[[All,2]]-min01;
```

Normalizing the decay curve.

```
data04[[All,2]]=data03[[All,2]]/Max[data03[[All,2]]];data04;
decay01=Drop[data04,{First[First[Position[data04,Min[data04]]]]}];
```

Resetting the decay curve time axis to start at zero.

```
time1=First[decay01[[All,1]]];
decay01[[All,1]]=decay01[[All,1]]-time1;
```

Setting the plot ranges.

```
rf=IntegerPart[First[decay01[[All,1]]]]-1;
rl=IntegerPart[Last[decay01[[All,1]]]]+1;
```

The variable, dl, is the curve fit variable for intensity, df, is the curve fit variable for time and, df2, is a curve fit variable for time from the non-normalized plot.

```
dl=Last[decay01[[All,2]]];
df=First[decay01[[All,1]]];
df2=First[decay01[[All,1]]];
min02=(Min[decay01[[All,2]]]);
decay01minzero=decay01;
```

Finding the best variable, c, for c+a(exp[-bx]).

```
min03=min02+(-.009);
```

Setting the data for best fit spread.

```
decay01minzero[[All,2]]=decay01[[All,2]]-min03;
min04=First[First[Position[decay01minzero[[All,2]],Min[decay01minzero[[All,2]]]]]];
decay02minzero=decay01minzero;
```

Dropping the value of zero so the empty set will not be generated when the natural log is taken on the data.

```
decay02minzero=Drop[decay02minzero,{min04}];
decay05=decay02minzero;
```

Taking the natural log of the data.

```
decay05[[All,2]]=Log[decay02minzero[[All,2]]]; decay05;
```

Setting up the residuals for future plots.

```
decay01residuals=decay05;
decay01residuals2=decay05;
decay01residuals3=decay05;
```

```
decay01residuals4=decay05;
decay01residuals5=decay01;
decay02=decay01[[All,2]];
decay06=decay02-min03;
min05=First[First[Position[decay06,Min[decay06]]]];
decay07=Drop[decay06,{min05}];
data05=Min[data[[All,2]]];
```

Normalizing the entire plot.

```
data06=data01;
data07=data01;
data06[[All,2]]=data[[All,2]]-data05;
data07[[All,2]]=data06[[All,2]]/Max[data06[[All,2]]];data07;
rl2=Last[data07[[All,1]]];
```

Plotting the data, the decay curve, and the natural log of the decay curve.

```
dplot01=ListPlot[data]
dplot02=ListPlot[decay01]
dplot03=ListPlot[decay05]
dplot04=ListPlot[data07,PlotRange→{{0,45},{0,1.1}},Frame→True,FrameLabel→{"
Time (ps)", "Intensity Normalized","Sample 2",None},RotateLabel→True]
```

Finding the linear curve fit using different weights.

```
(regress3=Regress[decay05,{1,x},x];Chop[regress3,10^(-6)])
(regress1=Regress[decay05,{1,x},x,Weights→√decay07 ];Chop[regress1,10^(-6)])
(regress2=Regress[decay05,{1,x},x,Weights→decay07];Chop[regress2,10^(-6)])
(regress4=Regress[decay05,{1,x},x,Weights→ (decay07)^2];Chop[regress4,10^(-6)])
datafit01=NonlinearRegress[decay01,dl+C11+A11*Exp[-B11*(x-
df)],{x},{A11,B11,C11}]

b1=regress1[[1,2,1,1,1]];
b2=regress2[[1,2,1,1,1]];
b3=regress3[[1,2,1,1,1]];
b4=regress4[[1,2,1,1,1]];
b5=datafit01[[2,2,1,1,1]];
m1=regress1[[1,2,1,2,1]];
m2=regress2[[1,2,1,2,1]];
m3=regress3[[1,2,1,2,1]];
m4=regress4[[1,2,1,2,1]];
m5=datafit01[[2,2,1,2,1]];
c11=datafit01[[2,2,1,3,1]];
```

Plotting the fit parameters.

```
func1[x_]=Fit[decay05,{1,x},x];
func2sqrt[x_]=b1+m1*x;
func3var[x_]=b2+m2* x;
func3sqrd[x_]=b4+m4*x;
func2[x_]=dl+c11+b5*Exp[-m5*(x-df)]
P1=Plot[func1[x],{x,rf,rl},DisplayFunction→Identity ,PlotStyle→RGBColor[0,1,0]]
P2=Plot[func2sqrt[x],{x,rf,rl},DisplayFunction→Identity,PlotStyle→RGBColor[0,1,1]]
P3=Plot[func3var[x],{x,rf,rl},DisplayFunction →Identity,PlotStyle→RGBColor[0,0,1]]
P4=Plot[func3sqrd[x],{x,rf,rl},DisplayFunction→Identity,PlotStyle→RGBColor[1,0,1]]
P5=Plot[func2[x],{x,rf,rl},DisplayFunction → Identity,PlotStyle→RGBColor[1,0,0]]
```

Comparing the curve fit with the data.

```
Show[dplot03,P1]
Show[dplot03,P2]
Show[dplot03,P3]
Show[dplot03,P4]
Show[dplot02,P5, PlotRange→All]

se1=regress1[[1,2,1,2,2]];
se2=regress2[[1,2,1,2,2]];
se3=regress3[[1,2,1,2,2]];
se4=regress4[[1,2,1,2,2]];
se5=datafit01[[2,2,1,2,2]];
set1=se1*(1/m1^2);
set2=se2*(1/m2^2);
set3=se3*(1/m3^2);
set4=se4*(1/m4^2);
set5=se5*(1/m5^2);
```

Finding the residuals.

```
For[i=1,i≤Length[decay05],decay01residuals[[i,2]]=decay05[[i,2]]-
func1[decay01minzero[[i,1]]];
  i++]
For[i=1,i≤Length[decay05],decay01residuals2[[i,2]]=decay05[[i,2]]-
func2sqrt[decay01minzero[[i,1]]];
  i++]
For[i=1,i≤Length[decay05],decay01residuals3[[i,2]]=decay05[[i,2]]-
func3var[decay01minzero[[i,1]]];
  i++]
For[i=1,i≤Length[decay05],decay01residuals4[[i,2]]=decay05[[i,2]]-
func3sqrd[decay01minzero[[i,1]]];
```

```
 i++]
For[i=1,i≤Length[decay01],decay01residuals5[[i,2]]=decay01[[i,2]]-
func2[decay01[[i,1]]];
 i++]
```

Plotting the residuals to verify if the fits are good.

```
ListPlot[decay01residuals]
ListPlot[decay01residuals2]
ListPlot[decay01residuals3]
ListPlot[decay01residuals4]
ListPlot[decay01residuals5]
```

Setting up for plot comparison between the fit and the data.

```
Decaynw=□^(-(x/(1/-m3))+b3)+min02;
Decaysqrt=□^(-x/(1/-m1)+b1)+min02;
Decayvar=□^(-x/(1/-m2)+b2)+min02;
Decaysqrd=□^(-x/(1/-m4)+b4)+min02;
DecayNL=dl+c11+b5*□^(-(x-df)/(1/m5));
dplot05=ListPlot[decay01,DisplayFunction → Identity]

PD1=Plot[Decaynw, {x,rf,rl} ,DisplayFunction→Identity,PlotStyle->RGBColor[0,1,0]]
PD2=Plot[Decaysqrt, {x,rf,rl},DisplayFunction→Identity,PlotStyle->RGBColor[0,1,1]]
PD3=Plot[Decayvar, {x,rf,rl},DisplayFunction→Identity,PlotStyle->RGBColor[0,0,1]]
PD4=Plot[Decaysqrd, {x,rf,rl},DisplayFunction→Identity,PlotStyle->RGBColor[1,0,1]]
PD5=Plot[DecayNL, {x,rf,rl},DisplayFunction→Identity,PlotStyle->RGBColor[1,0,0]]
PD6=Plot[DecayNL, {x,rf,rl},DisplayFunction→Identity]

Show[dplot05,PD1,DisplayFunction→$DisplayFunction,PlotRange→All,Frame→True
,FrameLabel→{"Decay Rates (ps)", "Intensity Normalized"},RotateLabel→True]
Show[dplot05,PD2,DisplayFunction→$DisplayFunction,PlotRange→All,Frame→True
,FrameLabel→{"Decay Rates (ps)", "Intensity Normalized"},RotateLabel→True]
Show[dplot05,PD3,DisplayFunction→$DisplayFunction,PlotRange→All,Frame→True
,FrameLabel→{"Decay Rates (ps)", "Intensity Normalized"},RotateLabel→True]
Show[dplot05,PD4,DisplayFunction→$DisplayFunction,PlotRange→All,Frame→True
,FrameLabel→{"Decay Rates (ps)", "Intensity Normalized"},RotateLabel→True]
Show[dplot05,PD5,DisplayFunction→$DisplayFunction,PlotRange→All,Frame□True,
FrameLabel→{"Decay Rates (ps)", "Intensity Normalized"},RotateLabel→True]
Show[dplot05,PD6,DisplayFunction→$DisplayFunction,PlotRange→All,Frame→True
,FrameLabel→{"Decay Rates (ps)", "Intensity
Normalized","Sample1",None},RotateLabel→True]
```

Double exponential decay $Ae^{-t/\tau_1} + Be^{-t/\tau_2}$

```
datafit02=NonlinearFit[decay01,dl+A*Exp[-B*(x-df)]+C1*Exp[-D1*(x-
df)],{x},{A,B,C1,D1}]
datafit03=NonlinearRegress[decay01,dl+A*Exp[-B*(x-df)]+C1*Exp[-D1*(x-
df)],{x},{A,B,C1,D1}]

bb1=datafit03[[2,2,1,2,1]];
dd1=datafit03[[2,2,1,4,1]];
sebb1=datafit03[[2,2,1,2,2]];
sedd1=datafit03[[2,2,1,4,2]];
```

Plotting the double exponential $Ae^{-t/\tau_1} + Be^{-t/\tau_2}$.

```
datafit04[y_]=datafit02/.x→y;
fitplt01=Plot[datafit04[x],{x,rf,rl},PlotStyle→RGBColor[1,0,0]]
```

Standard deviation from the calibration and the actual laser pulse width.

```
cg1=2.36863;
cg2=22.53541;
cg3=42.81046;
dis1=cg2-cg1-20;
dis2=cg3-cg2-20;
err1=(dis1+dis2)/2;
pulse1=.170;
```

The calculated lifetimes for the different fits.

```
sebbt1=sebb1*(1/bb1^2);
seddt1=sedd1*(1/dd1^2);
Lifetime=PlusMinus[1/-m3, √(set3^2+pulse1^2+err1^2) ]
Lifetimeweightedsqrt=PlusMinus[1/-m1, √(set1^2+pulse1^2+err1^2) ]
Lifetimeweightedvar=PlusMinus[1/-m2, √(set2^2+pulse1^2+err1^2) ]
Lifetimeweightedsqrd=PlusMinus[1/-m4, √(set4^2+pulse1^2+err1^2) ]
LifetimeNL=PlusMinus[1/m5, √(set5^2+pulse1^2+err1^2) ]
Lifetimebb1=PlusMinus[1/bb1, √(sebbt1^2+pulse1^2+err1^2) ]
Lifetimedd1=PlusMinus[1/dd1,√(seddt1^2+pulse1^2+err1^2) ]
```

Comparing the fit with the plot of the data.

```
Show[fitplt01,dplot02,PlotRange→All,Frame→True,FrameLabel→{"Decay Rates
(ps)", "Intensity Normalized"},RotateLabel→True]
```

Plot of the residuals for the double exponential $Ae^{-t/\tau_1} + Be^{-t/\tau_2}$.

```
decay01residualsee06=decay01;
decay08=decay01;
For[i=1,i≤Length[decay7],decay01residualsee06[[i,2]]=decay01[[i,2]]-
datafit01[decay08[[i,1]]]; i++]
ListPlot[decay01residualsee06]
```

Double exponential decay $(1-e^{-t/\tau_1})Ae^{-t/\tau_2}$.

```
datafit05=NonlinearFit[data07,dl+(1-Exp[-B*(x-df2)])*C1*Exp[-D1*(x-
df2)],{x},{B,C1,D1}]
datafit06=NonlinearRegress[data07,dl+(1-Exp[-(B*(x-df2))])*C1*Exp[-(D1*(x-
df2))],{x},{B,C1,D1}]
```

Lifetimes for the double exponential $(1-e^{-t/\tau_1})Ae^{-t/\tau_2}$.

```
bb3=datafit06[[2,2,1,1,1]];
dd3=datafit06[[2,2,1,3,1]];
sebb3=datafit06[[2,2,1,1,2]];
sedd3=datafit06[[2,2,1,3,2]];
sebbt3=sebb3*(1/bb3^2);
seddt3=sedd3*(1/dd3^2);
Lifetimebb3=PlusMinus[1/bb3, √(sebbt3^2+pulse1^2+err1^2 )]
Lifetimedd3=PlusMinus[1/dd3, √(seddt3^2+pulse1^2+err1^2 )]
```

Comparing the fit with the plot of the data.

```
fitplt02=Plot[datafit05,{x,df2,rl2},PlotStyle□RGBColor[0,0,1]]
Show[fitplt02,dplot04,PlotRange□All,Frame□True,Axes□ False,FrameLabel□{"Decay
Rates (ps)", "Intensity Normalized","Sample 1",None},RotateLabel□True]
```

Calling the image of the decay curve into Mathamatica.

```
s1imagetr101=Import["F:\Thesis\Lifetimes\Display Image\s1-150um-tr1-01.tif"]
Show[s1imagetr101,Frame□True,FrameLabel□{ None,"Time","Sample
1",None},RotateLabel□True,PlotRange□All ,
FrameTicks□{None,{{0,"45"},{48,""},{96,"36"},{144,""},{192,"27"},{240,""},{288,"1
8"},{336,""},{384,"9"},{432,""},{480,"0"}}}]
```

Bibliography

1. Bhattacharya, Pallab, *Semiconductor Optoelectronic Devices* (2nd Edition), New Jersey, Prentice Hall, 1997.

2. McKelvey, John P., *Solid State Physics for Engineering and Materials Science*, Florida, Krieger Publishing Company, 1993.

3. Pankove, Jacques., *Optical Processes in Semiconductors*, New York, Dover, 1975.

4. Jost, Thomas R., *Limitations in the Time Resolved Photoluminescence of Gallium Nitride Using a Streak Camera*, Thesis, Air Force Institute of Technology, May 2004

5. Department of Chemistry, Yale University. http://ursula.chem.yale.edu/~cas/ZnTe.html, Accessed 30 Aug 2005.

6. Hecht, Eugene., *Optics* (4th Edition), New York, Addison Wesley, 2002.

7. Cumblidge, Kevin. *Using Time-Resolved Photoluminescence to Measure the Excitation and Temperature Dependence of Carrier Relaxation in Mid-Wave Infrared Semiconductors*, Thesis, Air Force Institute of Technology, Feb 2004

8. H. Zhong, N. Karpowicz, J. Partridge, X. Xie, J. Xu, X. C. Zhang. *Terahertz Wave Imaging for Landmine Detection*, Proceedings of SPIE, 5411, 33, 2004.

9. M. J. Hagmann, B. A. McBride, Z. S. Hagmann. *Pulsed and Widely-Tunable Terahertz Sources For Security: Imaging and Spectroscopy*, Proceedings of SPIE, 5411, 51, 2004.

10. Z. Liliental-Weber, H.J. Cheng, S. Gupta, J. Whitaker, K. Nichols, and F.W. Smith, *Structure and Carrier Lifetime in LT-GaAs,* Journal of Electronic Materials, 22-12, 1465-1469, 1993.

11. F. Ganikhanov, J. M. Shieh, and C. L. Pan, *Dynamics of the Absorption Recovery of Dyes Commonly Used as Intracavity Saturable Absorbers in Self-Starting Passively Mode-Locked Ti:sapphire Lasers*, Optics Communications, 114, 289 (1995).

12. "Streak Camera Instruction Manual C6860: Operation Guide", Hamamatsu Photonics K.K. Sunayama-Cho, Japan. Not dated.

13. Hamamatsu Web Page. “Femtosecond Streak Camera Specifications.” http://usa.hamamatsu.com/assets/pdf/hpspdf/Femtosecond.pdf?GLBSESSID=589b816f18c140f0c52c7a9cf28ae7e2. Accessed 14 June 2004,

14. T. Korn, A. Franke-Wiekhorst, S. Schnull, and I. Wilke, *Characterization of nanometer AS-cluseter in low-temperature grown GaAs by transient reflectivity measurements*, Journal of Applied Physics, 91-4, 2333-2336 (February 2002).

15. Gorski, Steven M., *Carrier Dynamics in Mid-Infrared Quantum Well Lasers Using Time-Resolved Photoluminesence*. MS thesis, AFIT/GAP/ENP/02M-01. School of Engineering Physics, Air Force Institute of Technology (AU), Wright-Patterson AFB OH, March 2002.

16. F. Ganikhanov, G.-R. Lin, W.-C. Chen, C.-S. Cheng, and C.-L. Pan, *Subpicosecond carrier lifetimes in arsenic-ion-implanted GaAs,* Applied Physics Letter, 67-23, 3465-3467 (December 1995)

17. S. S. Prabhu and A. S. Vengurlekar, *Dynamics of the Pump-Probe Reflectivity Spectra in GaAs and GaN*, Journal of Applied Physics, 95-12, 7803-7811 (June 2004).

18. Verdeyen, Joseph T., *Laser Electronics*, 3rd ed. Prentice Hall, Upper Saddle River NJ, 1995.

19. R. L. Holtzapple, *Experimental Techniques for the CESR Streak Camera*, Laboratory of Nuclear Studies, Cornell University, Ithaca, New York, (CBN01-2)

20. D.F. Bliss, C. Lynch, D. Weyburne, K. O’Hearn, and J.S. Bailey, *Epitaxial Growth of Thick GaAs on Orientation-Patterned Wafers for NLO Applications*, Air Force Research Laboratory, Hanscom AFB, Massachusetts.

21. Johnson, Peter M., *Deviation of Time-Resolved Luminescence Dynamics in MWIR Semiconductor Materials from Carrier Recombination Theory Predictions*. Thesis, Air Force Institute of Technology, 2002.

REPORT DOCUMENTATION PAGE

Form Approved
OMB No. 074-0188

1. REPORT DATE *(DD-MM-YYYY)*	**2. REPORT TYPE**	**3. DATES COVERED** *(From – To)*
03-23-2006	**Master's Thesis**	Jun 2005 – Mar 2006

4. TITLE AND SUBTITLE

Carrier Lifetime Dynamics of Epitaxial Layer HVPE Gallium Arsenide Using Time-Resolved Experiments

5a. CONTRACT NUMBER

5b. GRANT NUMBER

5c. PROGRAM ELEMENT NUMBER

6. AUTHOR(S)

Wayne E. Eikenberry, Captain, USAF

5d. PROJECT NUMBER
06351

5e. TASK NUMBER

5f. WORK UNIT NUMBER

7. PERFORMING ORGANIZATION NAMES(S) AND ADDRESS(S)

Air Force Institute of Technology
Graduate School of Engineering and Management (AFIT/ENP)
2950 Hobson Way
WPAFB OH 45433-7765

8. PERFORMING ORGANIZATION REPORT NUMBER

AFIT/GAP/ENP/06-03

9. SPONSORING/MONITORING AGENCY NAME(S) AND ADDRESS(ES)

Dr. Walter Buchwald
Air Force Research Laboratory/SNHC
Hanscom AFB, MA 01731

Dr. Donald Silversmith
AFRL/AFOSR
4015 Wilson Blvd
Arlington, Va 22203-1954

10. SPONSOR/MONITOR'S ACRONYM(S)

11. SPONSOR/MONITOR'S REPORT NUMBER(S)

12. DISTRIBUTION/AVAILABILITY STATEMENT

APPROVED FOR PUBLIC RELEASE; DISTRIBUTION UNLIMITED.

13. SUPPLEMENTARY NOTES

14. ABSTRACT

GaAs is a potential semiconductor material for producing both mid-infrared and terahertz radiation using the new technique of quasi-phase matching in an orientationally patterned GaAs (OP-GaAs) crystal. OP-GaAs is grown using a fast growth process called hydride vapor phase epitaxy (HVPE), unfortunately, HVPE produces a high number of defects. These defects cause Shockley-Read-Hall recombination rates to dominate over Auger and radiative recombination rates. The carrier lifetime from four OP-GaAs samples are reported here using two different experimental techniques. The first experiment used a streak camera to measure the carrier lifetime via time-resolved photoluminescence. The temporal resolution of the streak camera can resolve the fast decay rate of the HVPE grown OP-GaAs samples. The carrier lifetimes recorded by the streak camera for sample one is 8.5 ± 0.3 ps, sample two is 8.4 ± 0.3 ps, sample three is 11.3 ± 0.3 ps, and sample four is 10 ± 0.3 ps. The second experiment used time-resolved pump-probe reflectivity to measure the carrier lifetime. This experiment used two laser beams; one was to excite the sample and the other was to measure the change in the index of refraction caused by the carrier excitation. The carrier lifetimes obtained by the pump-probe experiment for sample one is 0.8 ± 0.2 ps, sample two is 2.1 ± 0.2 ps, sample three is 3.8 ± 0.2 ps, and sample four is 1.3 ± 0.2 ps. The results of the lifetimes of these two experiment methods differ with each other.

15. SUBJECT TERMS

Semiconductors, Gallium Arsenide, Carrier Lifetime, Radiative Lifetime, Time Resolved Photoluminescence, Time Resolved Pump Probe Reflectivity, Shockley-Reed-Hall, Streak Camera

16. SECURITY CLASSIFICATION OF:			**17. LIMITATION OF ABSTRACT**	**18. NUMBER OF PAGES**	**19a. NAME OF RESPONSIBLE PERSON**
REPORT	**ABSTRACT**	**c. THIS PAGE**			Matthew J. Bohn, Lt Col, USAF AFIT/ENP.
U	**U**	**U**	**UU**	79	**19b. TELEPHONE NUMBER** *(Include area code)* (937) 255-6565, ext 4573; e-mail: Matthew.Bohn@afit.edu